Journal of Sound and Vibration 618 (2025) 119289

Contents lists available at ScienceDirect

Journal of Sound and Vibration

journal homepage: www.elsevier.com/locate/jsvi

Crowdsensing-based bridge vibration monitoring using a sparse network of random mobile sensors: Theory and numerical verifications

Mohammad Talebi-Kalaleh, Mustafa Gül, Qipei Mei *

Department of Civil and Environmental Engineering, University of Alberta, Edmonton, AB, Canada

ARTICLE INFO

Keywords:
Indirect bridge health monitoring
Vehicle scanning method
Drive-by SHM
Crowdsensing
Bridge condition monitoring
Smart infrastructure

ABSTRACT

Vibration monitoring of bridges is essential for the safety and maintenance of transportation infrastructure. Traditional methods rely on placing sensors directly on bridges, a process that is often costly and difficult to scale. An emerging alternative involves utilizing sensors mounted within vehicles as they traverse the bridge. However, this approach often faces challenges with continuous monitoring due to the limited time vehicles spend on the structure. This paper presents a novel framework for predicting bridge responses and identifying its modal characteristics through the crowdsensing of sparse vibration data from a network of vehicles traversing the bridge. The framework employs vehicles' body accelerations and positional data to estimate bridge responses at distributed virtual fixed sensing nodes (VFSNs). By randomly selecting some vehicles as sensing agents at sequential timestamps, it ensures a reliable and continuous flow of data. Additionally, the framework mitigates the influence of road roughness and vehicle dynamics by utilizing residual contact-point responses between the rear and front axles of the sensing vehicles. Simulations of a three-span bridge under realistic traffic conditions, including road roughness and vehicle–bridge interaction, were conducted to validate the framework's accuracy. Despite an 80% data missing rate and relying on only two sensing agents along with 17 VFSNs, the framework successfully identified the first three modes of the bridge with MAC values above 95% and natural frequencies with relative errors below 3%. Response predictions showed an accuracy exceeding 70%. Various factors were investigated, including traffic speed, the number of sensing agents and VFSNs, ambient noise effects, and the impact of the random vehicle selection process. The results confirmed the robustness of the framework against ambient noise and randomness in sensing agent selection. The optimal configuration was identified as two sensing agents and 17 VFSNs.

1. Introduction

Recent reports have highlighted the critical condition of municipal infrastructure in Canada, particularly concerning highway bridges. Canada has more than 50,000 bridges, most of which were constructed decades ago [1]. Over 40% of these bridges are now over 50 years old, with many facing structural or functional issues that necessitate costly repairs or replacements [2]. This issue is also evident in the United States, where many bridges built during the 1950s and 1960s are aging [3]. The 2019 Canadian Infrastructure Report Card shows that about 40% of Canadian bridges are rated as 'fair', 'poor', or 'very poor' [4], and nearly 9% of

* Corresponding author.
E-mail addresses: talebika@ualberta.ca (M. Talebi-Kalaleh), mustafa.gul@ualberta.ca (M. Gül), qipei.mei@ualberta.ca (Q. Mei).

https://doi.org/10.1016/j.jsv.2025.119289
Received 24 December 2024; Received in revised form 17 April 2025; Accepted 5 June 2025
Available online 20 June 2025

U.S. bridges are considered structurally deficient [5]. However, effective repairs demand continuous monitoring across the entire transportation network. Regular and continuous monitoring enables timely detection of structures in urgent need of attention. This not only prevents potential loss of lives and assets due to unexpected collapses but also supports proactive maintenance scheduling, thereby reducing maintenance and lifecycle costs. Ultimately, the adoption of intelligent monitoring solutions for infrastructure condition assessment is a crucial step toward realizing smart cities.

Traditional bridge condition monitoring systems often rely on fixed sensors installed directly on the structures, with subsequent data analysis to detect potential damages. These methods necessitate extensive equipment, substantial installation efforts, and the presence of numerous on-site experts [6–8]. While offering high accuracy and a degree of automation, such systems entail significant costs, require substantial time commitments, and may even necessitate bridge closures during sensor installation. These factors render them impractical for large-scale or nationwide structural monitoring projects. Consequently, many short- and medium-span bridges remain without Structural Health Monitoring (SHM) systems due to these practical, economic, and installation challenges [9].

Recent advancements have introduced drive-by monitoring methods, where sensors are mounted on vehicles to monitor bridge conditions. Known as drive-by or indirect bridge monitoring, these approaches provide a cost-effective and efficient solution [10]. First proposed by Yang et al. [11], this technique has significantly evolved [12]. Traditional drive-by methods primarily focus on identifying bridge natural frequencies, with fewer efforts dedicated to the identification of bridge mode shapes. Frequency identification typically involves analyzing the vehicle's acceleration response using the Fourier transform, complemented by filtering or transformation techniques like Wavelet and Hilbert transforms [13,14]. The identified frequencies can also be utilized for bridge damage detection [15,16]. Mode shape identification, crucial for structural engineering tasks such as Finite Element (FE) modal updating and damage detection, mainly relies on the theoretical response from the vehicle–bridge interaction (VBI). For a simply-supported bridge subjected to a quarter-car passage, this often involves using techniques like the short-time Fourier transform or the Hilbert transform on the vehicle's response [17,18]. Some approaches use the state–space representation of the VBI system [19–21] or apply Singular Value Decomposition (SVD) on the mapped responses [22,23]. These extracted mode shapes are also valuable for detecting potential damages [24,25].

The rapid evolution of Internet of Things (IoT) technologies has facilitated the integration of sensors into smart devices such as electric vehicles and smartphones [26,27]. This progress has led to the development of methods that utilize data from the accelerometers of smartphones in vehicles crossing bridges, as an alternative to professional sensors. Although this approach may not match the accuracy of professional sensors, it significantly reduces the cost of drive-by monitoring techniques [28]. Despite potential accuracy limitations, smartphone-based drive-by monitoring has become increasingly popular for identifying bridge frequencies and detecting structural damage [29]. The brief duration that a single vehicle spends crossing a bridge poses challenges in capturing sufficient vibration data to predict the bridge's behavior [30]. Some studies have suggested that data from multiple crossings by instrumented vehicles can address the issue of short data length and significantly improve the accuracy and reliability of bridge modal identification. This approach can be applied using multiple passages of a single instrumented vehicle [31] or by collecting smartphone data from various vehicles [32,33].

Utilizing a diverse range of data collected from smartphones in vehicles, known as crowdsensing-based bridge monitoring, represents the latest advancement in the field of indirect monitoring. So far, very little research has been conducted in this area. This method enables the collection of large-scale, real-time data for Structural Health Monitoring (SHM) applications [34]. The research group of the present authors [32,33] has introduced a crowdsensing-based methodology for detecting bridge damage using data from a large number of vehicles passing by. Their innovative approach has been validated through both numerical simulations and laboratory experiments, establishing a correlation between damage severity and feature magnitude. Matarazzo et al. [35] conducted a real-field experiment to evaluate the feasibility of crowdsensing-based bridge monitoring techniques. By utilizing smartphone data from everyday vehicle trips over bridges like the Golden Gate and a concrete bridge, including both controlled field experiments and uncontrolled Uber rides, they were able to accurately determine critical natural frequencies of the bridge, using smartphone data from different vehicle trips.

While crowdsensing-based methods show promise in terms of cost-effectiveness and scalability, this field is still nascent and faces several challenges. These include consistently capturing the vibrational characteristics of bridges under real-world traffic scenarios and complex bridge geometries, as well as mitigating the effects of road roughness. Another notable challenge is internet connectivity; vehicles may experience gaps in data transmission while crossing bridges, resulting in missing data. To overcome these obstacles, our study proposes a comprehensive crowdsensing-based framework designed to address the limitations of signal length in drive-by methods, the impacts of road roughness, and connectivity issues in existing crowdsensing-based bridge monitoring techniques. This approach utilizes acceleration and location data from a diverse network of sensing vehicles as they cross the bridge, enabling the prediction of bridge acceleration responses at various fixed virtual sensing nodes. To the best of the authors' knowledge, this article is the first to propose a framework that leverages a random network of mobile sensors from a population of vehicles through the concept of compressive sensing for continuous vibration monitoring of bridges. This includes predicting bridge responses and identifying mode shapes. Our method is unique in that it does not depend on any specific vehicle within the network and randomly samples from the pool of connected vehicles. It is also semi-data-driven, meaning it does not require a predefined model of the bridge. This provides a robust solution for continuous monitoring, utilizing the widespread availability and connectivity of smartphones in vehicles to ensure accurate and timely assessments of bridge health. A key innovation of our practical and cost-effective monitoring solution is the introduction of a random mobile sensing framework for compressed sensing of bridge vibration data. The selection of sensing agents in our framework may vary from one moment to the next, reflecting real-world conditions where vehicles may intermittently lose or regain internet connectivity. Additionally, we introduce a systematic approach to predict bridge vibration responses using the residual CP response, further enhancing the method's effectiveness and reliability.

The structure of this paper is organized as follows: After the introduction in this section, Section 2 provides a comprehensive description of the proposed methodology. Section 3 details the numerical simulations conducted on a three-span bridge under traffic flow. Section 4 presents the results of the proposed indirect monitoring framework, focusing on the prediction of bridge responses and its modal characteristics. Section 5 explores the influence of various factors on the accuracy of the framework. Finally, Section 6 concludes the paper by summarizing the key findings, discussing the limitations, and suggesting potential avenues for future research.

2. Methodology

This research introduces a methodology aimed at predicting bridge responses and identifying modal properties. Utilizing a network of randomly selected vehicles equipped with sensors, the proposed framework harnesses location data, vehicle vibration responses, and optimization techniques to enhance indirect bridge monitoring. The methodology is structured into several key steps to improve the translation of vibration data from vehicles to bridge responses:

- **First Step:** The framework begins by mapping measured vehicle body responses, which inherently include the vehicle's mechanical properties, to tire-level responses. This mapping is crucial for filtering out mechanical frequencies from the recorded signals.
- **Second Step:** The next step involves addressing the corruption of absolute Contact-Point (CP) responses of the axles, which are typically marred by noisy, stochastic road roughness. By employing residual CP responses, the framework aims to eliminate the effects of road roughness.
- **Third Step:** Finally, the residual CP responses, which still contain the vehicle's driving frequency, are projected onto Virtual Fixed Sensing Nodes (VFSNs) strategically positioned on the bridge. This projection is essential for effectively filtering out the driving frequencies. The final signals will be free from the vehicle's mechanical and driving frequencies, as well as the road roughness, ideally containing only the bridge vibrations.

Fig. 1 outlines the steps of the proposed framework. Location data from nearby internet-connected vehicles is used to create a list of vehicle IDs. From this list, m vehicles on the bridge are selected as sensing agents. These agents collect and transmit vertical acceleration, pitch rotation, and location data via a network. The agents' mechanical and dimensional properties are retrieved from a database, and rear axle locations are calculated using this data combined with their location data. The average speed of the agents is estimated to determine the time lag of the axles. The agents are then ordered by their rear axle location, and residual CP acceleration responses are calculated. These responses are compiled into a vector, forming the residual mobile sensing vector. VFSNs are selected based on bridge geometry, and a mapping matrix is generated using the axle positions and VFSNs. Solving a regularized optimization problem with this matrix and the mobile sensing vector yields the bridge's acceleration response derivative (jerk) at the VFSNs.

2.1. Symbols and definitions

Table 1 provides a comprehensive list of key symbols and their definitions, which are utilized in this section.

2.2. Contact-point response of sensing vehicles

In this study, we adopt the half-car (HC) model, as illustrated in Fig. 2(a), to replicate vehicles traversing the bridge. This model, commonly utilized in vehicle dynamics analysis, offers a simplified yet effective representation [36]. Considering a vehicle equipped with rigid tires and disregarding the mass contribution of the tires relative to the vehicle body, we can use the simplified version of the HC model [37].

For the vehicle depicted in Fig. 2(a) with a wheelbase of d, if a sensor is placed at a distance of e_s from the front axle, capable of measuring the vertical body response and pitch rotation of the vehicle body at the sensor location ($y_s(t)$ and $\theta_s(t)$), the vehicle's body response and pitch rotation at its center of gravity ($y_v(t)$ and $\theta_v(t)$) can be obtained under the assumption that the vehicle body is rigid. Given that the center of gravity of the vehicle is located at e_f from the front axle or e_r from the rear axle ($e_r + e_f = d$), this can be achieved using a linear relationship:

$$\mathbf{y}(t) = \mathbf{T}\mathbf{y}_s(t) \tag{1}$$

where $\mathbf{y}(t) = \begin{bmatrix} y_v(t) & \theta_v(t) \end{bmatrix}^\top$ represents the vector of vehicle responses at the center of gravity, and $\mathbf{y}_s(t) = \begin{bmatrix} y_s(t) & \theta_s(t) \end{bmatrix}^\top$ denotes the vector of vehicle responses at the sensor location. $\mathbf{T}$ is a transformation matrix that can be determined using the following equation:

$$\mathbf{T} = \begin{bmatrix} 1 & -(e_f - e_s) \\ 0 & 1 \end{bmatrix} \tag{2}$$

Defining the input vector as $\mathbf{u}_c(t) = \begin{bmatrix} u_{cr}(t) & u_{cf}(t) \end{bmatrix}^\top$, the equation of motion for the vehicle can be derived using principles of structural dynamics. Further details about the derivation steps can be found in [36,37]:

$$\mathbf{M}\ddot{\mathbf{y}}(t) + \mathbf{C}\dot{\mathbf{y}}(t) + \mathbf{K}\mathbf{y}(t) = \mathbf{B}_k\mathbf{u}_c(t) + \mathbf{B}_c\dot{\mathbf{u}}_c(t) \tag{3}$$

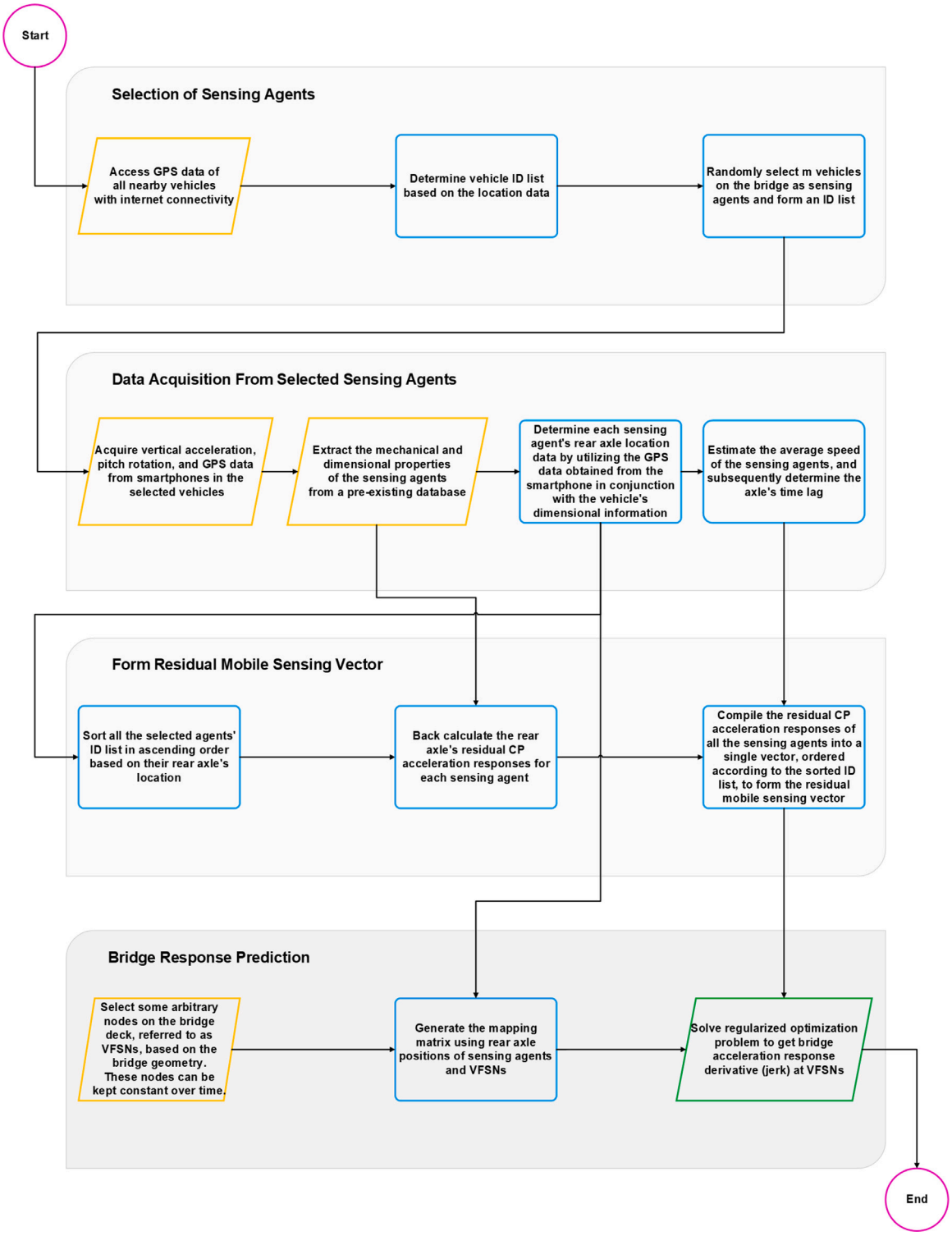

Fig. 1. The proposed crowdsensing-based framework for bridge response estimation using a network of random mobile sensors.

Table 1
List of symbols and their descriptions used in this paper.

Symbol	Description
d	Wheelbase of the vehicle
v	Speed of the vehicle
e_s	Distance from the front axle to the sensor location
e_f	Distance from the front axle to the vehicle's center of gravity
e_r	Distance from the rear axle to the vehicle's center of gravity
$y_s(t), \theta_s(t)$	Vertical displacement and pitch rotation at the vehicle's sensor location
$\mathbf{y}_s(t)$	Displacement response vector at the vehicle's sensor location
$\mathbf{z}_s(t)$	Acceleration response vector at the vehicle's sensor location
$y_v(t), \theta_v(t)$	Vertical displacement and pitch rotation at the vehicle's center of gravity
$\mathbf{y}(t)$	Displacement response vector at the vehicle's center of gravity
$\mathbf{z}(t)$	Acceleration response vector at the vehicle's center of gravity
$\mathbf{T}$	Transformation matrix relating the vehicle's response vectors at the sensor location to those at the center of gravity
M_v, J_v	Vertical mass and mass moment of inertia of the vehicle, respectively
k_{sf}, c_{sf}	Suspension stiffness and damping at the front axle, respectively
k_{sr}, c_{sr}	Suspension stiffness and damping at the rear axle, respectively
$\mathbf{M}, \mathbf{C}, \mathbf{K}$	Mass, damping, and stiffness matrices of the vehicle
$\mathbf{B}_k, \mathbf{B}_c$	Load effect matrices related to stiffness and damping
$u_{cr}(t), u_{cf}(t)$	Contact point displacement responses at the vehicle's rear and front axles, respectively
$\mathbf{u}_c(t)$	Vector containing the vehicle's contact point displacement responses
$\mathbf{w}_c(t)$	Vector containing the vehicle's contact point acceleration responses
$\mathbf{\Psi}(t)$	Defined time function used in the vehicle input estimation equation
(j)	Superscript indicating variables associated with the jth sensing agent
$u_{mr}(t), u_{mf}(t)$	Bridge responses at the locations of the vehicle's rear and front axles
$\ddot{\mathbf{u}}_m(t)$	Vector containing acceleration responses of the bridge at the locations of both the front and rear axles of all vehicles at time t
$r_r(t), r_f(t)$	Road roughness profile at the location of the rear and front axle
Δt	Time lag between the front and rear axles for the vehicle
$\Delta u_{cr}(t)$	Residual contact point response at the rear axle
$\Delta u_{mr}(t)$	Residual bridge response at the rear axle
$x_s(t)$	Recorded location data for the vehicle
$x_r(t), x_f(t)$	Determined rear and front axle locations of the vehicle
$\mathbf{L}(t)$	Mapping matrix that interpolates bridge responses from Virtual Fixed Sensing Nodes (VFSNs) to Mobile Sensing Nodes (MSNs) at time t
$\mathbf{L}_r(t)$	Rear-specific mapping matrix that interpolates bridge responses at the rear axle locations of vehicles at time t
$\ddot{\mathbf{u}}_b(t)$	Vector representing the hypothetical acceleration responses of the bridge recorded at the VFSNs at time t
$\mathbf{N}(x)$	Interpolating function vector used in mapping matrices to interpolate responses across spatial locations on the bridge
λ	Regularization parameter used in optimization problems
$\mathbf{\Gamma}(t)$	Random measurement matrix at time t indicating which VFSNs are actively recording responses
$\ddot{\mathbf{w}}_b(t)$	Complete acceleration response vector (true response) of the bridge at time t
T_d	Total measurement time of the signals
$\mathbf{\Phi}$	Mode shape matrix of the bridge
$\ddot{\mathbf{Q}}(t)$	Modal coordinate response vector at time t
$\mathbf{G}(\omega)$	Cross/auto power spectrum (CPSD) matrix of the response signals at frequency ω
$\mathbf{\Sigma}_i$	Diagonal matrix of singular values obtained from the SVD of $G(\omega)$, representing modal energy at frequency ω_i
$\mathbf{U}_i, \mathbf{V}_i$	Matrices of the left and right singular vectors from the SVD of $G(\omega)$, representing the mode shapes at frequency ω_i

where $\mathbf{M}, \mathbf{C}$, and $\mathbf{K}$ are the mass, damping, and stiffness matrices of the vehicle, respectively, while $\mathbf{B}_k$ and $\mathbf{B}_c$ represent the load effect matrices. These matrices for the HC model can be calculated as follows [36]:

$$\mathbf{M} = \begin{bmatrix} M_v & 0 \\ 0 & J_v \end{bmatrix}, \quad \mathbf{C} = \begin{bmatrix} c_{sr} + c_{sf} & e_f c_{sf} - e_r c_{sr} \\ e_f c_{sf} - e_r c_{sr} & e_r^2 c_{sr} + e_f^2 c_{sf} \end{bmatrix}, \quad \mathbf{K} = \begin{bmatrix} k_{sr} + k_{sf} & e_f k_{sf} - e_r k_{sr} \\ e_f k_{sf} - e_r k_{sr} & e_r^2 k_{sr} + e_f^2 k_{sf} \end{bmatrix} \tag{4}$$

$$\mathbf{B}_k = \begin{bmatrix} k_{sr} & k_{sf} \\ -e_r k_{sr} & e_f k_{sf} \end{bmatrix}, \quad \mathbf{B}_c = \begin{bmatrix} c_{sr} & c_{sf} \\ -e_r c_{sr} & e_f c_{sf} \end{bmatrix} \tag{5}$$

Here, M_v and J_v represent the vehicle's vertical mass and mass moment of inertia, respectively. $u_{cr}(t)$ and $u_{cf}(t)$ denote the CP inputs to the vehicle's rear and front axles, respectively. k_{sf} and c_{sf} are the suspension stiffness and damping of the front axle, while k_{sr} and c_{sr} represent the suspension stiffness and damping of the rear axle.

In practice, measuring displacements directly is often not feasible. Instead, it is much easier to measure the angular acceleration and vertical acceleration of the vehicle body at a random location on the vehicle using smartphone sensors or commercially-graded accelerometers. To express Eq. (3) in terms of accelerations or their derivatives at the sensor location, one can differentiate both sides of the equation twice and then substitute $\ddot{\mathbf{y}}(t) = \mathbf{z}(t) = \mathbf{T}\mathbf{z}_s(t)$ from Eq. (1), which relates the acceleration at the vehicle's center of gravity ($\mathbf{z}(t)$) with the accelerations measured at a random location by a sensor ($\mathbf{z}_s(t)$). Additionally, we need to substitute $\ddot{\mathbf{u}}_c(t) = \mathbf{w}_c(t)$, which is the CP acceleration responses of the vehicle. Thus, we obtain:

$$\mathbf{M}\mathbf{T}\ddot{\mathbf{z}}_s(t) + \mathbf{C}\mathbf{T}\dot{\mathbf{z}}_s(t) + \mathbf{K}\mathbf{T}\mathbf{z}_s(t) = \mathbf{B}_k\mathbf{w}_c(t) + \mathbf{B}_c\dot{\mathbf{w}}_c(t) \tag{6}$$

As previously discussed, the vehicle body response $\mathbf{z}_s(t)$ can be accurately measured at any location on the vehicle using either smartphones or commercial accelerometers. The first and second derivatives of $\mathbf{z}_s(t)$ are computed through numerical differentiation.

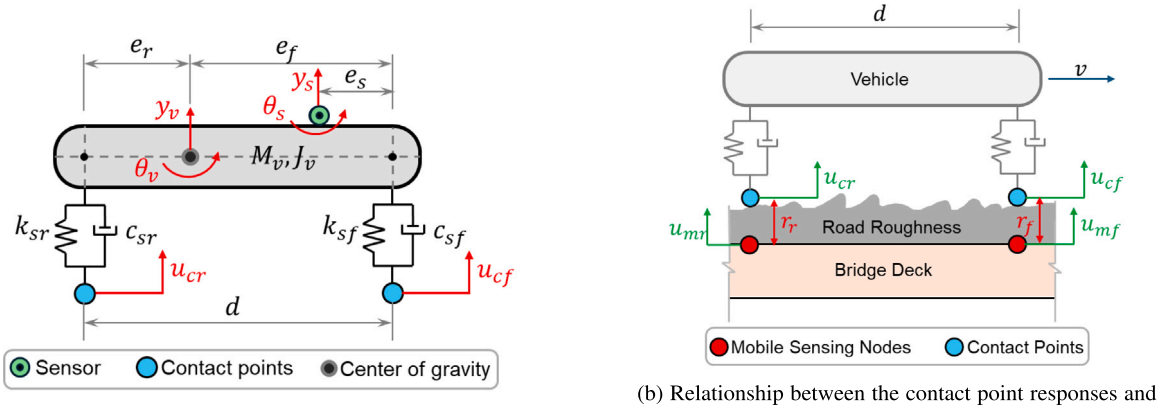

(a) Parameters of the vehicle

(b) Relationship between the contact point responses and the bridge responses at the vehicle's axles' locations

Fig. 2. Parameters of the Half-Car model and illustration of road roughness effect on the vehicle scanning methods.

Given known mechanical properties, such as suspension stiffness, damping, and body mass, all relevant vehicle matrices can be determined. Consequently, the left-hand side of Eq. (6) becomes a defined time function, represented by $\mathbf{\Psi}(t)$. This setup leads to the formulation of a first-order system of equations:

$$\mathbf{B}_c\dot{\mathbf{w}}_c(t) + \mathbf{B}_k\mathbf{w}_c(t) = \mathbf{\Psi}(t) \tag{7}$$

Since $\mathbf{\Psi}(t)$ is solely a function of vehicle properties and the vertical and rotational responses of the vehicle body measured at the sensor location, we can solve this system of first-order differential equations for the CP acceleration vector $\mathbf{w}_c(t)$ explicitly using Duhamel's formula [38] or using a numerical method, as both $\mathbf{B}_k$ and $\mathbf{B}_c$ are known.

$$\mathbf{w}_c(t) = \left\{ \begin{array}{c} \ddot{u}_{cr}(t) \\ \ddot{u}_{cf}(t) \end{array} \right\} = \int_0^t e^{-(\mathbf{B}_c^{-1}\mathbf{B}_k)(t-\tau)}\mathbf{B}_c^{-1}\mathbf{\Psi}(\tau)d\tau \tag{8}$$

The primary objective of determining the vehicles' CP responses is to filter out the mechanical frequencies of the vehicle included in the measured body responses [39]. However, the new signals still encompass the driving frequencies of the vehicles.

It is important to highlight that, in this study, we proceed with the assumption that CP responses can be directly computed using the Eq. (8) derived earlier, given vehicle parameters and body rotation alongside vertical responses. However, obtaining complete datasets for vehicle mechanical properties based on vehicle types can be challenging in practice. Recent research has explored methods for identifying vehicle properties. One approach involves accessing the vehicle's body responses before it enters the bridge and optimizing vehicle parameters by minimizing the difference between identified front and rear road profiles on a short, constant-speed road section using optimization techniques such as genetic algorithm [40]. Another method employs on-bridge responses of the vehicle directly in a joint input-parameter estimate to identify CP roughnesses and vehicle properties using the extended Kalman filter with unknown inputs (EKF-UI) algorithm [41,42]. Additionally, the "frequency-free" movable test vehicle approach in [43] could further reduce vehicle-induced frequency contamination if a specialized, stiff-suspension vehicle were deployed in parallel.

2.3. Eliminating road roughness effects using residual CP responses

Previous studies [39] have indicated that vehicle scanning methods are highly sensitive to the bridge surface roughness. This sensitivity arises because the vehicle senses not only the bridge response at the MSNs but also the bridge response corrupted by the road roughness profile, as depicted in Fig. 2(b). The following equations represent the relationship between the CP responses of the jth sensing agent ($u_{cr}^{(j)}(t)$ or $u_{cf}^{(j)}(t)$), the bridge response at the position of the vehicle's rear or front axles of the sensing agent ($u_{mr}^{(j)}(t)$ or $u_{mf}^{(j)}(t)$), and the road roughness profile at the location of the front or rear axle of the sensing agent ($r_r^{(j)}(t)$ or $r_f^{(j)}(t)$):

$$u_{cr}^{(j)}(t) = u_{mr}^{(j)}(t) + r_r^{(j)}(t) \tag{9}$$

$$u_{cf}^{(j)}(t) = u_{mf}^{(j)}(t) + r_f^{(j)}(t) \tag{10}$$

To mitigate such negative effects, an effective approach is to adopt the residual CP responses of the rear and front axle. The surface roughness effect can be inherently eliminated using residual CP responses, even for damped bridges with rough pavements [39]. This approach was initially demonstrated effectively using a 1-DOF quarter-car model [44]. It was later successfully tested with 2-DOF quarter-car [45] and half-car models [46]. Additionally, the relationships between vehicle body and CP responses were investigated using a single sensor with the quarter-car model [42]. To address the challenges of using connected vehicles in practical applications, Yang et al. [47] proposed eliminating vehicle frequencies and road roughness by using residual CP responses from a single vehicle,

a method validated with a 2-DOF half-car model. He and Yang [48] suggested that the residual acceleration spectrum at the contact points of a single two-axle vehicle can be used to identify the bridge's frequencies with high accuracy.

Considering the wheelbase of $d^{(j)}$ and a constant speed of $v^{(j)}$ for the selected sensing agent, since the rear and front tires of the vehicle sense the same roughness but with a lag of $\Delta t^{(j)} = v^{(j)}/d^{(j)}$, the following transparent relationship can be considered between the roughness inputs of the front and rear axles [49].

$$r_r^{(j)}(t) = r_f^{(j)}(t - \Delta t^{(j)}) \tag{11}$$

By substituting $(t - \Delta t^{(j)})$ for t in Eq. (10) and then substituting Eq. (11) into it, we obtain:

$$u_{cf}^{(j)}(t - \Delta t^{(j)}) = u_{mf}^{(j)}(t - \Delta t^{(j)}) + r_r^{(j)}(t) \tag{12}$$

Now, subtracting Eq. (9) from Eq. (12), we can define the residual CP response at the position of the rear axle for the jth sensing agent as follows:

$$\Delta u_{cr}^{(j)}(t) = u_{cr}^{(j)}(t) - u_{cf}^{(j)}(t - \Delta t^{(j)}) = u_{mr}^{(j)}(t) - u_{mf}^{(j)}(t - \Delta t^{(j)}) = \Delta u_{mr}^{(j)}(t) \tag{13}$$

As seen, $\Delta u_{cr}^{(j)}(t)$ exhibits an exceptional roughness-free feature and the Residual CP response of the rear axle is free from the road roughness high frequencies and is exactly equal to the residual responses at the MSNs. However, obtaining the absolute response of the bridge using the residual MSN response remains a challenging task, which is addressed in Section 2.4.

2.4. Bridge response prediction using mobile sensors

Consider a scenario where a population of vehicles is traversing a bridge. At an arbitrary time t, the CP responses of m sensing vehicles referred to as sensing agents, are accessible. Utilizing location data collected simultaneously with the CP responses for the sensing agents, denoted as $x_s^{(j)}(t)$ for the jth sensing agent, enables the determination of the rear and front axle locations of each vehicle ($x_r^{(j)}(t)$ and $x_f^{(j)}(t)$) as follows:

$$\begin{aligned} x_r^{(j)}(t) &= x_s^{(j)}(t) + e_s^{(j)} - d^{(j)}, \\ x_f^{(j)}(t) &= x_s^{(j)}(t) + e_s^{(j)}, \end{aligned} \tag{14}$$

where $e_s^{(j)}$ and $d^{(j)}$ represent the distances between the sensor position and the front axle, and the wheelbase of the jth sensing agent, respectively [50].

To maintain the method's generality, we first consider an ideal scenario in which the bridge surface is completely smooth. In this scenario, the response of the contact points aligns perfectly with the bridge response at the positions of the vehicle's rear or front axles, which we denote as Mobile Sensing Nodes (MSNs). In a broader context, if we measured the bridge response at n arbitrary Virtual Fixed Sensing Nodes (VFSNs) properly distributed along the bridge, we could effectively determine the bridge response at the mobile sensing nodes using a mapping function $\mathbf{L}(t)$. This process entails interpolating the responses recorded at the VFSNs and their respective positions on the bridge relative to its left support (s_i), as illustrated in Fig. 3 [50].

$$\ddot{\mathbf{u}}_m(t) = \mathbf{L}(t)\ddot{\mathbf{u}}_b(t) \tag{15}$$

where $\ddot{\mathbf{u}}_m(t)$ is a $(2m \times 1)$ vector containing acceleration responses of the bridge at the locations of both the front and rear axles of all sensing agents, and $\ddot{\mathbf{u}}_b(t)$ is an $(n \times 1)$ vector representing the acceleration responses of the bridge hypothetically recorded at the VFSNs.

$$\ddot{\mathbf{u}}_m(t) = \left[\ddot{u}_{mr}^{(1)}(t) \quad \ddot{u}_{mf}^{(1)}(t) \quad \cdots \quad \ddot{u}_{mr}^{(m)}(t) \quad \ddot{u}_{mf}^{(m)}(t)\right]^\top \tag{16}$$

$$\ddot{\mathbf{u}}_b(t) = \left[\ddot{u}_b^{(1)}(t) \quad \ddot{u}_b^{(2)}(t) \quad \cdots \quad \ddot{u}_b^{(n-1)}(t) \quad \ddot{u}_b^{(n)}(t)\right]^\top \tag{17}$$

The mapping matrix $\mathbf{L}(t)$ is a $(2m \times n)$ matrix, where each row represents the transpose of the interpolating function vectors $\mathbf{N}(x)$ corresponding to each MSN location. In this study, we assume the interpolating function vector to be linear.

$$\mathbf{L}(t) = \left[\mathbf{N}\left(x_r^{(1)}(t)\right) \quad \mathbf{N}\left(x_f^{(1)}(t)\right) \quad \cdots \quad \mathbf{N}\left(x_r^{(m)}(t)\right) \quad \mathbf{N}\left(x_f^{(m)}(t)\right)\right]^\top \tag{18}$$

$$\mathbf{N}^\top(x) = \begin{matrix} s_1 & \cdots & s_i & s_{i+1} & \cdots & s_n \end{matrix} \\ \begin{bmatrix} 0 & \cdots & \frac{x - s_{i+1}}{s_i - s_{i+1}} & \frac{x - s_i}{s_{i+1} - s_i} & \cdots & 0 \end{bmatrix} \tag{19}$$

In indirect bridge monitoring methods, the responses at the MSNs ($\ddot{\mathbf{u}}_m(t)$) are actual measurements obtained from the sensing agents, while the response of the bridge at the VFSNs ($\ddot{\mathbf{u}}_b(t)$) remains unknown. To predict the bridge response at the VFSNs, the mapping matrix $\mathbf{L}(t)$ is utilized along with a regularized least-squares optimization problem:

$$\min_{\ddot{\mathbf{u}}_b} \|\mathbf{L}\ddot{\mathbf{u}}_b - \ddot{\mathbf{u}}_m\|^2 + \lambda\|\ddot{\mathbf{u}}_b\|^2 \tag{20}$$

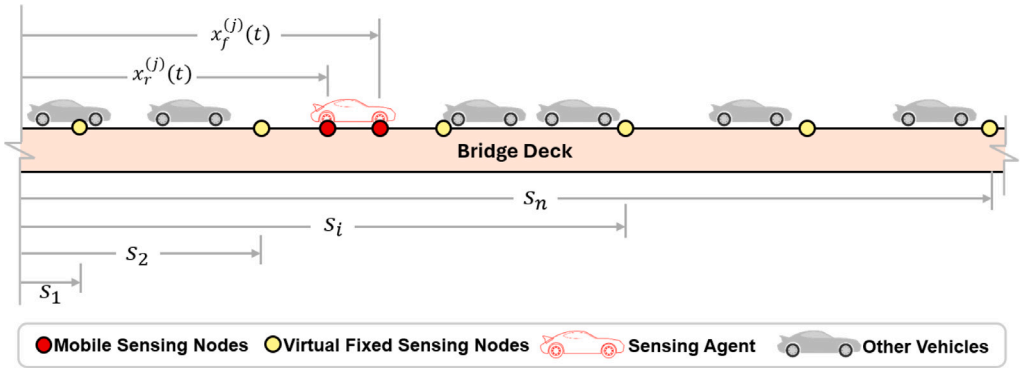

Fig. 3. Illustrative figure for Mobile Sensing Nodes and Virtual Fixed Sensing Nodes.

Here, λ represents the regularization parameter, and $\|\ddot{\mathbf{u}}_b\|^2$ denotes the Euclidean norm, quantifying the sum of squares of the vector's elements. The solution to this optimization problem is given by:

$$\ddot{\mathbf{u}}_b(t) = (\mathbf{L}^\top(t)\mathbf{L}(t) + \lambda\mathbf{I})^{-1}\mathbf{L}^\top(t)\ddot{\mathbf{u}}_m(t) \tag{21}$$

The derivation of the above equation in our approach is independent of any assumptions about bridge properties, making it a semi-data-driven, model-free method. Extending the previously established mapping procedure for scenarios without road roughness, we now incorporate road roughness into the analysis. First, the MSN responses at the front and rear axles are evaluated using Eq. (15). To simplify the analysis and establish a clear relationship between residual CP responses and bridge response, here we assume a constant time lag for all sensing agents ($\Delta t^{(j)} = \Delta t$). While the proposed method accommodates variable speeds and wheelbases of sensing agents, this simplification ensures a uniform time step across all sensing agents. Importantly, this assumption does not restrict the speeds of other vehicles on the bridge, and the method remains effective under variable traffic conditions. By shifting time (t) to ($t - \Delta t$) for the MSNs at the front axle location of all sensing agents, while considering $x_f^{(j)}(t - \Delta t^{(j)}) = x_r^{(j)}(t)$, we obtain:

$$\ddot{\mathbf{u}}_{mr}(t) = \mathbf{L}_r(t)\ddot{\mathbf{u}}_b(t) \tag{22}$$

$$\ddot{\mathbf{u}}_{mf}(t - \Delta t) = \mathbf{L}_r(t)\ddot{\mathbf{u}}_b(t - \Delta t) \tag{23}$$

$$\mathbf{L}_r(t) = \left[\mathbf{N}\left(x_r^{(1)}(t)\right) \quad \cdots \quad \mathbf{N}\left(x_r^{(m)}(t)\right)\right]^\top \tag{24}$$

where the interpolation function vector $\mathbf{N}(x)$ was defined before. and $\ddot{\mathbf{u}}_{mr}(t)$ and $\ddot{\mathbf{u}}_{mf}(t)$ are the vectors containing the rear and front axle response of all the sensing agents at the MSNs, respectively. $\ddot{\mathbf{u}}_b(t)$ and $\ddot{\mathbf{u}}_b(t - \Delta t)$ are the bridge response vector at time step t and $(t - \Delta t)$ respectively.

$$\Delta\ddot{\mathbf{u}}_{mr}(t) = \left[\Delta\ddot{u}_{mr}^{(1)}(t) \quad \cdots \quad \Delta\ddot{u}_{mr}^{(m)}(t)\right]^\top \tag{25}$$

$$\Delta\ddot{\mathbf{u}}_b(t) = \left[\Delta\ddot{u}_b^{(1)}(t) \quad \cdots \quad \Delta\ddot{u}_b^{(n)}(t)\right]^\top \tag{26}$$

As can be seen, when using the residual response, the number of MSNs equals the number of sensing agents. By subtracting Eq. (23) from Eq. (22), dividing both sides of the resulting equation by Δt, and utilizing the second derivative of the residual CP responses in Eq. (13), a relationship between the residual CP responses of the vehicles and the bridge response can be derived:

$$\frac{\Delta\ddot{\mathbf{u}}_{mr}(t)}{\Delta t} = \mathbf{L}_r(t)\frac{\ddot{\mathbf{u}}_b(t) - \ddot{\mathbf{u}}_b(t - \Delta t)}{\Delta t} \tag{27}$$

If we assume that Δt is small enough, the fraction on the right-hand side of the aforementioned equation can be intuitively considered as the first approximate derivative of the acceleration response vector (jerk) of the bridge at time t:

$$\dot{\ddot{\mathbf{u}}}_b(t) \approx \frac{\ddot{\mathbf{u}}_b(t) - \ddot{\mathbf{u}}_b(t - \Delta t)}{\Delta t} \tag{28}$$

Given this approximation, we now have the same least squares optimization problem as in Eq. (20). In a similar manner, the derivative of the bridge acceleration response vector can be explicitly determined using the following equation:

$$\dot{\ddot{\mathbf{u}}}_b(t) \approx (\mathbf{L}_r^\top(t)\mathbf{L}_r(t) + \lambda\mathbf{I})^{-1}\mathbf{L}_r^\top(t)\left(\frac{\Delta\ddot{\mathbf{u}}_{mr}(t)}{\Delta t}\right) \tag{29}$$

Where λ is the regularization parameter. As seen in the derivation steps, using the residual CP acceleration responses of the sensing agents results in predicting the first derivative of the acceleration response vector of the bridge. This is typically a signal with

high-frequency components. To identify the acceleration response vector of the bridge, it is more effective to utilize the residual CP velocity response of the sensing agents:

$$\ddot{\mathbf{u}}_b(t) \approx (\mathbf{L}_r^{\top}(t)\mathbf{L}_r(t) + \lambda \mathbf{I})^{-1}\mathbf{L}_r^{\top}(t)\left(\frac{\Delta \dot{\mathbf{u}}_{mr}(t)}{\Delta t}\right) \tag{30}$$

After computing $\ddot{\mathbf{u}}_b(t)$ at each time step and arranging the responses of all p time steps into the columns of a larger matrix (each column corresponding to one time step), denoted as $\ddot{\mathbf{D}}$, the spatio-temporal acceleration response matrix of the bridge ($n \times p$). In this study, the regularization parameter, λ, is set to 10^{-6}. It is worth noting that the inverse mapping procedure, facilitated by the optimization framework, inherently filters out the effects of the vehicles' driving frequencies from the MSN signals. Consequently, the resulting bridge signals are free from these frequencies. Up to this step, we have filtered out the vehicles' mechanical and driving frequencies, as well as the road roughness frequencies. The remaining signals thus contain only the bridge's vibration response.

In this work, the inverse mapping from residual CP responses to VFSNs is formulated in Eqs. (29) and (30). However, for each time step t, certain VFSNs may lie outside the effective interpolation range of the sensing agents' axles, making the matrix $\mathbf{L}_r(t)$ nearly singular or yielding large errors. To address this, we only regard a VFSN as 'validly scanned' at time t if $\mathbf{L}_r(t)$ contains at least two nonzero entries in the corresponding column (assuming a linear shape function). This ensures that each node is anchored by sufficient local axle coverage to yield a stable solution. Algorithm 1 illustrates how we implement this rule within the framework. At time t, we examine each node's column in $\mathbf{L}_r(t)$: if the node has at least two nonzero entries, we mark it as valid by setting the corresponding diagonal element of the indicator matrix $\mathbf{\Gamma}(t)$ to 1. Otherwise, it remains 0. As a result, the spatio-temporal response matrix is populated only where the mobile sensing agents genuinely provide stable information about bridge vibration. Any node–time cells that fail this criterion flagged as missing.

Algorithm 1 Valid region identification in the spatio-temporal matrix for a given time stamp.

Require: $\mathbf{L}_r(t)$: mapping matrix from CP responses to VFSNs at time t.
Require: $\{x_r^{(j)}(t)\}$: rear axle positions of m sensing agents at time t.
Require: $\{s_i\}_{i=1,\dots,n}$: positions of the n VFSNs along the bridge.
Ensure: $\mathbf{\Gamma}(t)$: an $n \times n$ indicator matrix reflecting the validity of each VFSN at time t.

```
Γ(t) ← 0 {Initialize an n × n matrix of zeros.}
for each node s_i do
    Count how many nonzero entries appear in column i of L_r(t).
    if (the number of nonzero entries for s_i) ≥ 2 then
        Set the (i, i) entry of Γ(t) to 1.
    else
        Leave the (i, i) entry of Γ(t) as 0.
    end if
end for
return Γ(t)
```

It should be highlighted that classical drive-by SHM frameworks often assume constant vehicle speed, but the proposed approach can accommodate variable speeds and minor accelerations by combining accurate position estimation with the proposed contact-point response mapping procedure. Building on past researches [51,52], one can fuse the measured accelerometer data with GPS/magnetometer measurements to track the vehicle's position precisely. After mapping body-level signals to CP responses to remove low-frequency vehicle effects, these CP signals are projected onto fixed bridge nodes (VFSNs) using the accurate vehicles' position data. This final step filters out any driving frequencies resulting from speed changes or braking, leaving the bridge signals largely free of vehicle-induced distortions. Consequently, our method supports reliable modal identification under non-constant speeds.

2.5. Random mobile sensing method

In mobile sensing methods, one may opt for employing a single constant sensing vehicle over time, which constitutes the primary focus of conventional vehicle scanning methods [50,53]. With this approach, the vehicle can only capture the bridge's vibrations at VFSNs for a very brief period. As a result, the vibration signals recorded are very short, leading to a highly incomplete spatio-temporal response matrix ($\ddot{\mathbf{D}}$). The response matrix exhibits a diagonal population pattern [54], reflecting the movement and positions of the sensing vehicle (see Fig. 4(a)). This pattern, known as block-out missing data, can significantly increase errors in the modal identification process [55]. Alternatively, employing multiple constant sensing vehicles, where each vehicle crosses the bridge sequentially, can provide longer vibration signals at VFSNs, resulting in a continuous monitoring approach. Present crowdsensing-based indirect monitoring methodologies for bridge structures primarily adopt this strategy [33,34,56]. However, real-world challenges such as intermittent internet connections for vehicles crossing the bridge may arise. Even with the multi-passage approach, using constant agents over time can still result in a measurement matrix with block-out missing patterns (see Fig. 4(b)). This poses a significant challenge for data imputation and response completion methods, as a higher number of non-random missing components in the matrix can make its inversion singular. Therefore, devising a solution that does not rely on specific sensing

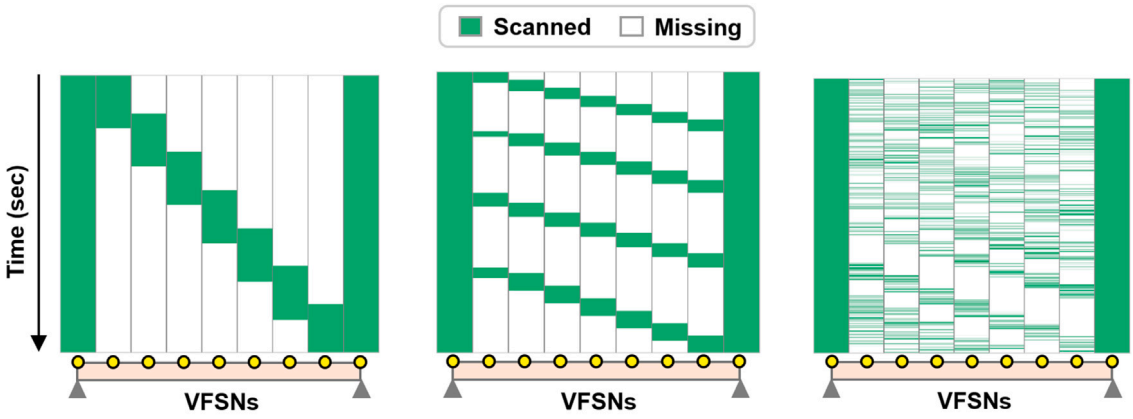

(a) Single passage of a constant sensing vehicle (classical drive-by methods).

(b) Multiple full passages of constant or different sensing vehicle(s).

(c) Continuous scanning using random sensing agents.

Fig. 4. Visual representation of scanned and missing regions in the spatio-temporal response matrix of the bridge (transposed) under different mobile sensing scenarios.

vehicles could represent a transformative advancement in crowdsensing-based SHM. In this study, we propose using random sensing agents at each time stamp, which leads to a measurement matrix characterized by Missing-At-Random (MAR) patterns. This approach can be more reliable in addressing issues of internet and data loss since it dynamically changes the sensing agent from one time step to the next. The measurement matrix generated from random mobile sensing (see Fig. 4) resembles a random sampling of the bridge and aligns with the principles of compressed sensing. As a result, this methodology enhances the fidelity of data collection by ensuring diverse coverage of the bridge's response over time.

2.6. Practical considerations for implementing the proposed method

While this paper primarily focuses on presenting the theoretical framework of the proposed method and validating its effectiveness using numerically simulated data, the practical considerations outlined in this section aim to facilitate its successful implementation on real bridges. This implementation is the future objective planned by the authors.

The proposed method estimates bridge responses for a specific lane based on sensing vehicles traveling in that lane. For larger bridges with multiple lanes, independent sensing setups can be employed for each lane. Vehicles are categorized by their lateral coordinates, allowing the estimation of bridge responses specific to each lane. For example, with three lanes, bridge responses can be estimated at the center of each lane, analogous to having three continuous lines of fixed sensors. While dense response measurements are achievable longitudinally, only a limited number of sensing lanes can be considered transversely. Modal identification can then be conducted independently for each sensing lane to extract the bridge's bending modes. If torsional modes are of interest, data from multiple sensing lanes can be aggregated and analyzed collectively. Given that vehicles may deviate laterally from the centerline of a sensing lane, the wheel-level responses must be mapped to the sensing lane's centerline (Fig. 5). Linear interpolation can be applied to align the responses of both wheels of an axle to an average value corresponding to the sensing lane.

It is important to note that the proposed method is not necessarily designed for real-time monitoring due to practical challenges associated with achieving real-time functionality. Instead, the method is well-suited for continuous monitoring over timeframes ranging from hours to days. This approach involves equipping sensing vehicles with a smartphone app that records acceleration and GPS data when vehicles enter the defined geographical boundary of a bridge. The data are stored locally on the user's device and are deleted after a predefined period (e.g., 24 h). During this window, if internet connectivity is available, data can be transmitted to a central server upon request. The server identifies vehicles present on the bridge during each timestamp and randomly selects some of them as sensing agents, then sends data requests to their respective devices, and receives a limited set of acceleration and GPS values rather than the entire dataset. The same vehicle may be selected as a sensing agent in subsequent timeframes.

Although our results in this study are based on ideal simulation data, we outline potential real-world approaches to time synchronization. When multiple sensing agents record data simultaneously, a unified smartphone app can label the data (e.g., acceleration and GPS) using a global clock derived from the device's GNSS receiver or a synchronized network service [34,52]. This step ensures all sensed values share a consistent time reference. At regular intervals (e.g., every 0.01 s or 0.02 s during post-processing), a central server requests a small window of data from each agent. By linearly interpolating each agent's measurements onto the server's common time grid, once can align potentially asynchronous signals. Measurements from sensors with delays exceeding a threshold (e.g., 0.2 s) are discarded to minimize the inclusion of significantly late or misaligned data. The general synchronization process is illustrated in Fig. 6 for two sensing agents. In scenarios involving a single sensing vehicle, synchronization is inherently simpler, requiring only one data point per timestamp.

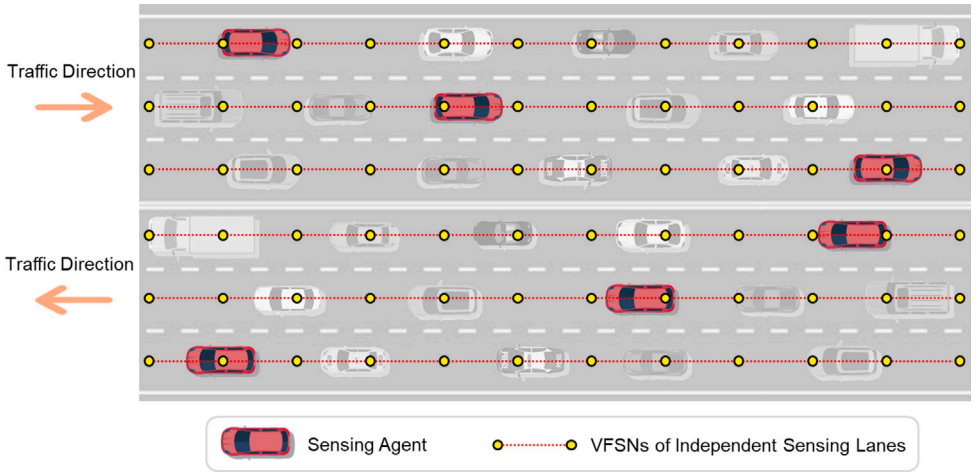

Fig. 5. Bridge response estimation at independent parallel sensing lanes.

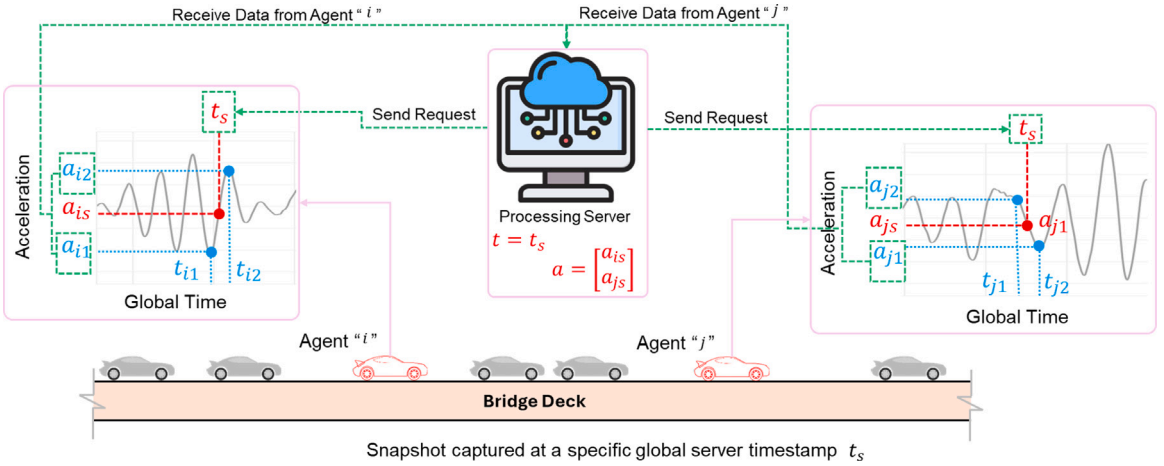

Fig. 6. Schematic representation of data synchronization from multiple random sensing agents via global timestamps and interpolation.

It should be highlighted that minor time offset typically occur but do not materially impact the estimation of structural mode shapes or natural frequencies. Previous studies confirm that standard Global Navigation Satellite System (GNSS) or Network Time Protocol (NTP)-based synchronization provides sufficient accuracy for vehicle-induced vibration analysis [35,57,58]. While we do not implement these algorithms in the current paper, future field validations will test the feasibility of the proposed interpolation-based timestamping of multiple sensing agents at global timestamps shown in Algorithm 2.

Once valid data from multiple agents are synchronized at a given global timestamp, one can fuse the data using Eqs. (29) and (30) to estimate bridge responses at the VFSNs. The random selection of agents further ensures continuity: if data from one agent are unavailable at a particular time, others fill the gap. Therefore, the proposed framework remains robust against typical data loss and delay scenarios in practical crowdsensing deployments [34,57].

2.7. Modal identification using the predicted responses with random missing regions

To identify the mode shapes through the predicted acceleration response matrix of the bridge, the Frequency Domain Decomposition method (FDD) is employed [59]. The procedure of applying FDD for the predicted acceleration response matrix with missing values is presented in the following paragraph. If we assume that $\ddot{\mathbf{w}}_b(t)$ is the complete response vector (true response) of the bridge at time t, and what we predicted for the bridge response using random mobile sensors with missing values is $\ddot{\mathbf{u}}_b(t)$, and since we know which represents which regions within the bridge is being scanned, let us define the random measurement matrix $\mathbf{\Gamma}(t)$ which is an $(n \times n)$ contains zeros and ones, ones correspond to the scanned VFSNs at each time step, thereby the following relationship between the complete and incomplete response vectors is as follow:

$$\ddot{\mathbf{u}}_b(t) = \mathbf{\Gamma}(t)\ddot{\mathbf{w}}_b(t) \tag{31}$$

Algorithm 2 Interpolation-Based Synchronization of Multiple Sensing Agents.

Require: Data_j: time-stamped measurements from agent j, $j = 1, \dots, M$.
Each Data_j contains $\{t_j(n), a_j(n)\}$ for $n = 1, \dots, N_j$.
Require: $\{t_k\}_{k=1}^{K}$: the server's global time grid.
Ensure: Synchronized signals $\tilde{a}_j(t_k)$ for $j = 1, \dots, M$ and $k = 1, \dots, K$.
for $j = 1$ to M **do**
  for $k = 1$ to K **do**
    Identify nearest time points $t_j(n_1)$, $t_j(n_2)$ around t_k.
    Interpolate to compute $\tilde{a}_j(t_k)$ from $a_j(n_1)$, $a_j(n_2)$.
    if $|t_j(n_i) - t_k| >$ threshold **then**
      discard $\tilde{a}_j(t_k)$ {Data point is too delayed.}
    end if
  end for
end for

From statistics, the correlation matrix between the incomplete response of the VFSNs can be constructed using Eq. (32) :

$$\mathbf{R}_{\ddot{\mathbf{u}}_b\ddot{\mathbf{u}}_b}(\tau) = \frac{1}{T_d}\int_0^{T_d} \ddot{\mathbf{u}}_b(t)\ddot{\mathbf{u}}_b^{\top}(t-\tau)dt = \begin{bmatrix} R_{\ddot{u}_b^{(1)}\ddot{u}_b^{(1)}}(\tau) & \cdots & R_{\ddot{u}_b^{(1)}\ddot{u}_b^{(n)}}(\tau) \\ \vdots & \ddots & \vdots \\ R_{\ddot{u}_b^{(n)}\ddot{u}_b^{(1)}}(\tau) & \cdots & R_{\ddot{u}_b^{(n)}\ddot{u}_b^{(n)}}(\tau) \end{bmatrix} \tag{32}$$

where T_d is the total measurement time of the signals.

Considering the modal expansion of the complete bridge response vector ($\ddot{\mathbf{w}}_b(t) = \boldsymbol{\Phi}\ddot{\mathbf{Q}}(t)$) in which $\boldsymbol{\Phi}$, $\ddot{\mathbf{Q}}(t)$ are mode shape matrix and modal coordinate response vector, respectively which are unknown. substituting the modal expansion in Eq. (32) gives:

$$\mathbf{R}_{\ddot{\mathbf{u}}_b\ddot{\mathbf{u}}_b}(\tau) = \frac{1}{p}\int_0^{p} \boldsymbol{\Phi}\ddot{\mathbf{Q}}(t)\ddot{\mathbf{Q}}^{\top}(t-\tau)\boldsymbol{\Phi}^{\top}dt = \boldsymbol{\Phi}\mathbf{R}_{\ddot{q}\ddot{q}}(\tau)\boldsymbol{\Phi}^{\top} \tag{33}$$

Then, taking the Fourier transform from both sides of the latter equation produces the matrix containing the cross/auto power spectrum (CPSD) of the response signals:

$$\mathbf{G}_{\ddot{q}\ddot{q}}(\omega_i) = \boldsymbol{\Phi}\mathbf{G}_{\ddot{q}\ddot{q}}(\omega_i)\boldsymbol{\Phi}^{\top} \tag{34}$$

$$\mathbf{G}_{\ddot{q}\ddot{q}}(\omega_i) = \mathbf{U}_i\boldsymbol{\Sigma}_i\mathbf{V}_i^{\top} \tag{35}$$

As can be understood from Eqs. (34) and (35), the SVD of matrix $\mathbf{G}_{\ddot{q}\ddot{q}}(\omega_i)$ should be calculated for each frequency, ω_i, in which the matrix of singular values ($\boldsymbol{\Sigma}_i$) is a diagonal matrix containing modal Frequency Response Functions (FRFs) and each column of the matrix of singular vectors ($\mathbf{U}_i$ and $\mathbf{V}_i$) represents the mode shapes corresponding to the given frequency ω_i.

3. Numerical simulation of bridge subjected to traffic flow

3.1. Bridge model

A numerical model of a three-span girder bridge, spanning 100 m as depicted in Fig. 7, was constructed using the finite element software OpenSees [60]. The bridge features a rectangular cross-section measuring 3 m in width and 1.5 m in height, with material properties assigned based on concrete, having a density of 2400 kg/m^3 and an elastic modulus of 27.5 GPa [32]. Employing 100 finite elements, the bridge underwent dynamic vehicle–bridge interaction analysis, utilizing the uncoupled iterative algorithm [61], a common method for such problems. Eigenvalue analysis revealed natural frequencies of 1.44 Hz, 3.68 Hz, and 4.66 Hz for the first three modes, respectively. For dynamic analysis, a 0.5% damping ratio was applied to the first and second modes of the bridge using the proportional damping model. Vertical and angular accelerations of vehicles, along with their location data, were sampled at a rate of 200 Hz from sensors mounted on the vehicle's body, positioned 0.5 m from the front axle.

3.2. Vehicle models

The vehicles were simulated using 2DOF Half-Car models, incorporating a diverse range of mechanical properties. Initial vehicle parameters were derived from the two-axle test vehicle proposed by Yang et al. [37]. It should be noted that while this study utilized models only based on the test vehicle, the application of our method is not limited to specific vehicle types. Indeed, the method can be adapted to any vehicle with varied parameters. The base parameters for the vehicle depicted in Fig. 2(a) included suspension stiffness values of 230 kN/m for the front axle (k_{fr}) and 180 kN/m for the rear axle (k_{sr}), a body mass (M_v) of 2500 kg, and a pitch moment of inertia (J_v) of 2300 kg m^2. Notably, no suspension damping was factored into the test vehicle's characteristics. In the traffic flow simulations, 30 vehicles are assumed. For all these vehicles, mechanical properties were randomly assigned within ranges

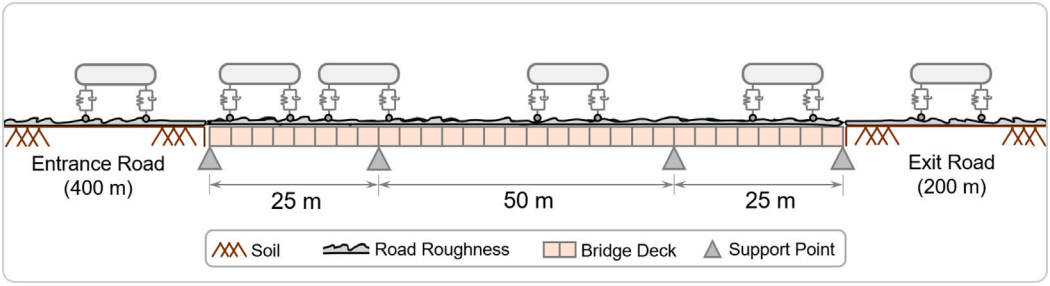

Fig. 7. Numerical model of the vehicle–bridge system subjected to the traffic flow of HC vehicles (considering road roughness).

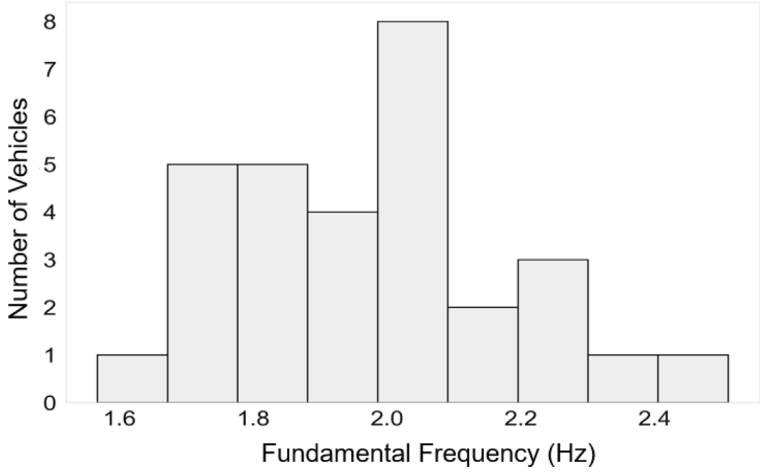

Fig. 8. Statistical distribution of bounce frequency for the 30 vehicles used in the simulations.

of 70% to 130% of those specified for the base vehicle, following a Gaussian distribution [62]. The wheelbase (d) was uniformly set at 3 m for all vehicles, and their base speed was assumed to be 90 km/h (25 m/s). Fig. 8 illustrates the statistical distribution of the fundamental frequencies for the vehicles used in the simulations. These varied mechanical properties are critical for a comprehensive representation of real-world vehicle dynamics in vehicle–bridge interaction analysis. Since the traffic scenario involves 30 vehicles with diverse mechanical properties, with the number of vehicles on the bridge changing over time, The identification of the bridge's modal properties is based on signals recorded during these varying conditions, allowing the method's performance to be assessed under random traffic scenarios. Furthermore, while the primary investigations assume constant vehicle speeds, Section 5.7 explores the influence of varying speeds within the traffic network.

3.3. Vehicle–bridge interaction and random traffic flow generation procedure

The iterative uncoupled method was considered [61] for the dynamic analysis of the vehicle–bridge system. The Iterative Vehicle–Bridge Interaction (VBI) Procedure (Algorithm 3) aims to achieve converged vehicles' contact forces and bridge responses given the mechanical properties and initial conditions for both bridge and vehicles. Initially, a FE model for the bridge is generated with adequate mesh density. Subsequently, 30 distinct 2D FE models are defined for the Half-Car vehicles with fixed bases. Location data for the front and rear axles of each vehicle over time are generated based on their constant speed (v) and initial location $(x_r^{(j)}(t), x_f^{(j)}(t))$, alongside road roughness input for each axle derived from the road roughness profile and vehicles' location data $(r_r^{(j)}(t), r_f^{(j)}(t))$. The iterative process begins with estimating the initial contact forces of the vehicles ($\mathbf{f}^{(j)}(t)$) and continues until convergence criteria are met. Within each iteration, dynamic analyses are performed on both the bridge model and each vehicle's FE model. The bridge response vector $\mathbf{w}_b(t)$ at time t and the bridge responses at the locations of the vehicles' axles $(u_{mr}^j(t))$ and $(u_{mf}^j(t))$ are determined. Notably, these responses are set to zero for vehicles not currently on the bridge. Then, the base inputs of the vehicles at time t are updated, and one-step forward dynamic analyses of each vehicle's FE model are conducted. The updated base reactions (contact forces) of the vehicles at time t are extracted and utilized to update the forces vector applied to the bridge. This process iterates until convergence, with the bridge model reanalyzed and its responses at time t recalculated based on the updated contact forces. Convergence criteria are evaluated at the end of each iteration, ensuring the accuracy and stability of the VBI procedure. In the VBI simulations, wheel–bridge contact was modeled at a single point, with the assumption that the vehicles'

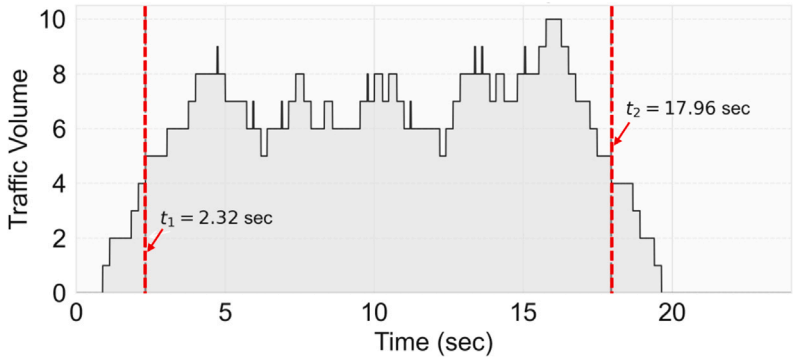

Fig. 9. Number of vehicles on the bridge over time and measurement running span.

contact forces would remain vertical. This simplification streamlines the analysis process while maintaining a focus on the essential aspects of the vehicle–bridge interaction. In order to replicate a consistent traffic flow scenario on the bridge, recommendations outlined in [63] were followed, assuming ideal traffic conditions without traffic jams or lane changes. 30 vehicles in total were generated 400 m before the bridge at random locations following a uniform distribution [62]. By monitoring the fluctuation in traffic volume over time, as delineated in Fig. 9, we could ascertain the establishment of a steady traffic flow pattern. Once this stability was observed, data collection commenced and persisted until a substantial dataset was amassed from the bridge, spanning a total duration of 15.64 s.

Algorithm 3 Iterative Vehicle-Bridge Interaction (VBI) Procedure.

Require: Mechanical properties and Initial conditions for bridge and vehicles
Ensure: Converged vehicles' contact forces and bridge responses

Generate a finite element model for the bridge with sufficient mesh density.
Define 30 separate 2D FE models for the HC vehicles with fixed bases.
Generate location data for the front and rear axles of each vehicle over time based on their initial location $\{x_r^{(j)}(t), x_f^{(j)}(t)\}$.
Generate road roughness input for each axle of vehicles based on the road roughness profile and vehicles' location data $\{r_r^{(j)}(t), r_f^{(j)}(t)\}$.
for $t = 1$ to T_d **do**
  Estimate initial contact forces of the vehicles $\{\mathbf{f}^{(j)}(t)\} \leftarrow \{\mathbf{f}^{(j)}(t-1)\}$
  while convergence criteria not met **do**
    Perform one-step forward dynamic analysis on the bridge model using the estimated contact forces $\{\mathbf{f}^{(j)}(t)\}$
    Obtain the bridge response vector at time t, $\mathbf{w}_b(t)$
    Determine bridge responses at the locations of the vehicle axles at time t, $\{u_{mr}^{j}(t)\}$ and $\{u_{mf}^{j}(t)\}$ (set to zero for off-bridge vehicles)
    for each vehicle j **do**
      Determine base inputs of the vehicle at time t $\{r_r^{(j)}(t) + u_{mr}^{(j)}(t), r_f^{(j)}(t) + u_{mf}^{(j)}(t)\}$
      Perform one-step forward dynamic analysis of vehicle jth FE model at time t subjected to the base excitation
      Extract the updated base reactions (contact) forces of the vehicle at time t $\{\mathbf{f}^{(j)}(t)\}$
    end for
    Update the forces vector being applied to the bridge using the on-bridge vehicles' contact forces at time t
    Reanalyze the bridge model and determine its responses at time t based on the updated contact forces
    Calculate convergence criteria
  end while
end for

3.4. Road roughness modeling

Road roughness is simulated by the method presented in ISO 8608 using a predefined PSD function [64]. The procedure can be represented by the following equations:

$$r(x) = \sum_{i=1}^{N} \sqrt{2G_d(\eta_i)\Delta\eta}\cos(2\pi\eta_i x + \theta_i) \tag{36}$$

$$G_d(\eta_i) = G_d(\eta_0)(\eta_i/\eta_0)^{-2} \tag{37}$$

Table 2
Road roughness classification (A–E) (Adapted from [64]).

Class	Description	Lower limit	Geometric mean	Upper limit
A	Very good	–	16	32
B	Good	32	64	128
C	Average	128	256	512
D	Poor	512	1024	2048
E	Very poor	2048	4096	8192

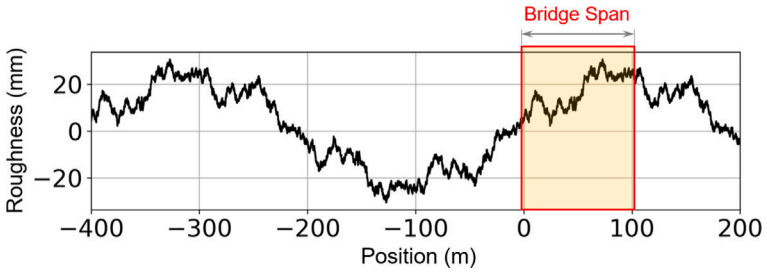

Fig. 10. The generated road roughness for class A road type.

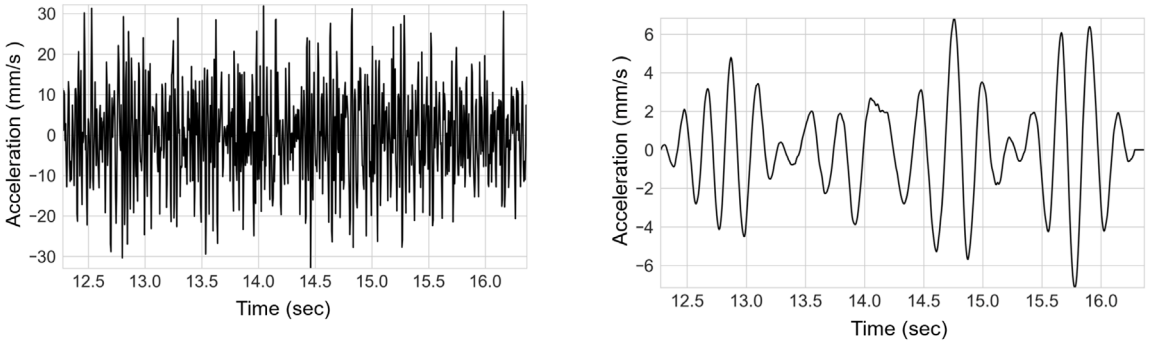

(a) Absolute CP response. (b) Residual CP response.

Fig. 11. Absolute CP and residual CP acceleration response of a sample vehicle while crossing the bridge considering road roughness.

where; $r(x)$ is the generated road roughness profile, θ_i is a random number uniformly distributed between 0 and 2π. $\Delta\eta$ is the sampling interval of the spatial frequency and is 0.01 cycle/m, and η_i is set a number in the range from 0.01 to 10 m^{-1} with an interval of $\Delta\eta$. $G_d(\eta_0)$ should be selected based on the class of road roughness. (See Table 2.)

In this research, the roughness class is assumed to be class A considering a very good condition for the road and the generated profile is shown in Fig. 10. It should be noted that the road profile generated for the 400 m road segment before the bridge along with the bridge span to have non-zero vibration for the vehicles before entering as well as better simulate the real-life traffic scenarios.

3.5. Numerical simulation results

As previously discussed, only the vertical acceleration and pitch rotation of the vehicles were recorded. The CP responses and the residual CP responses of the axles were derived using the vehicle properties and the back-calculation method outlined in Section 2.2. Figs. 11(a) and 11(b) present the absolute and residual CP responses of a sample vehicle's rear axle during the interval in which it crossed the bridge. The absolute CP response is significantly influenced by road roughness, rendering it unsuitable for predicting bridge responses. Conversely, the residual CP response, devoid of roughness effects, is more appropriate for such predictions. However, this response still retains the driving frequency of the vehicle, which must be filtered out using the technique proposed in Section 2.4.

4. Results of the random mobile sensing framework

For all the investigations, the base settings include 17 VFSNs and two selected sensing agents, assuming Class A road surface roughness unless specified otherwise. The impact of employing multiple sensing agents and varying the number of VFSNs will be

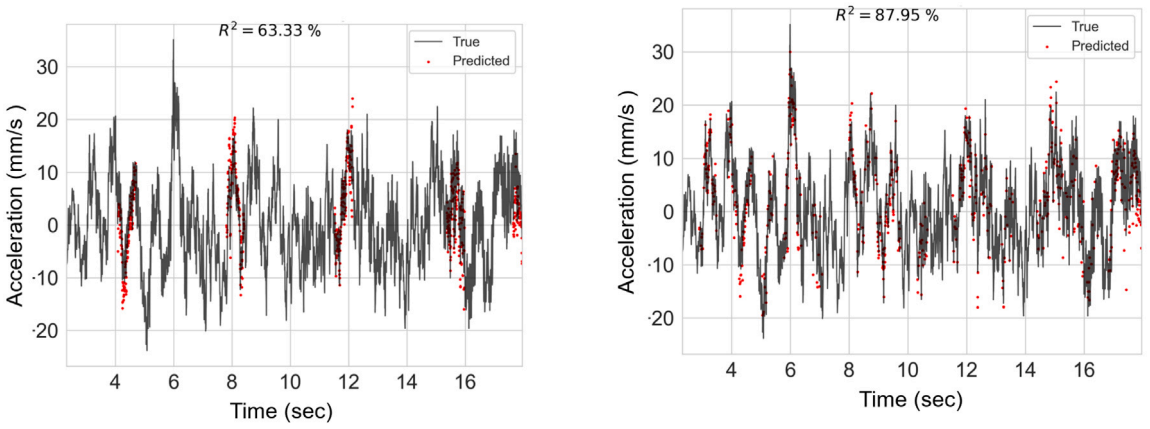

(a) Constant over time sensing agents.

(b) Random sensing agents.

Fig. 12. Predicted acceleration response of the bridge at a sample midspan VFSN for two different sensing agent selection scenarios (without road roughness).

explored in Section 5. Measurement noise is temporarily omitted in this analysis but will be addressed in the same section later. It is important to note that to determine bridge acceleration responses under conditions of road roughness, the velocity responses of vehicles were utilized to calculate residual CP responses, as discussed in 2.4.

4.1. Bridge response prediction

Based on the assumed measurement time window, the framework enables the determination of vibration responses at VFSNs across the bridge. To explore the impact of using either constant sensing agents or random sensing agents, Fig. 12 compares the bridge acceleration response predicted at the mid-span VFSN, disregarding road roughness in the simulations. The results demonstrate that using random sensing agents enables thorough scanning of important parts of the signals, leading to a compressed representation of the vibration data. This compressed scanning contributes significantly to condensing the signal representation and improves prediction accuracy (enhanced by 25% compared to the constant-agent case), effectively addressing the challenge of singular inverse solutions [50]. Conversely, utilizing constant agents over time limits signal prediction to short windows of scanned regions, potentially missing responses in certain time-windows. It is important to note that in the comparison presented in Fig. 12, only one sensing agent is used at each time stamp.

Returning to the main simulations involving road roughness, Figs. 13(a) and 13(b) compare the predicted acceleration responses of the bridge at two sample VFSNs against the true values. The results indicate that using the residual velocity response from random sensing agents provides reasonably accurate predictions (above 70%) for the bridge acceleration responses. Although these predictions are less accurate compared to simulations without road roughness, it becomes evident later that the framework's predicted responses contribute to higher accuracies in modal identifications. Notably, the magnitude of the bridge acceleration responses is significantly amplified compared to simulations without road roughness, primarily due to the inclusion of high-frequency components in the synthetic road roughness profile. Additionally, Fig. 13(c) illustrates the variation of the R^2 values for all the VFSNs over length, indicating that the accuracy of the predictions is consistent across all VFSNs, with an average accuracy of around 70%.

4.2. Modal identification

By setting the missing values in the predicted acceleration response matrix to zero and performing FDD on it (refer to Section 2.7), the modal frequencies can be easily identified from the first singular value of the PSD matrix (Fig. 14(a)). Following the FDD steps, the mode shapes can also be identified. A comparison of the identified mode shapes and the true mode shapes is presented in Fig. 14(b). As shown, the Modal Assurance Criterion (MAC) of the first three identified mode shapes of the bridge exceeds 95%, indicating the high accuracy of the framework. Additionally, Table 3 presents a comparison of the identified natural frequencies with the true values. While the relative error for the first mode shape is 2.2%, the errors for the remaining modal frequencies are less than 1%. This observation aligns with expectations because higher frequency vibrations are more easily discernible from acceleration measurements, whereas lower frequency components are better identified from displacement measurements [59]. This indicates that the accuracy of modal identification using the response matrix with randomly missing regions remains high. In contrast, results from a single-sensing-agent-based method are typically much lower [50].

It should be noted that the true mode shapes and natural frequencies were extracted from the numerical model in OpenSees by performing an eigenvalue analysis. The comparison between the true and identified natural frequencies and mode shapes is based on the following metrics:

$$\text{Relative Frequency Error} = \frac{|f_{\text{true}} - f_{\text{identified}}|}{f_{\text{true}}} \times 100 \tag{38}$$

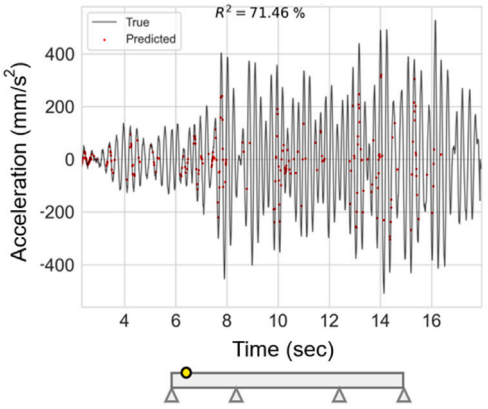

(a) A sample VFSN close to the left support.

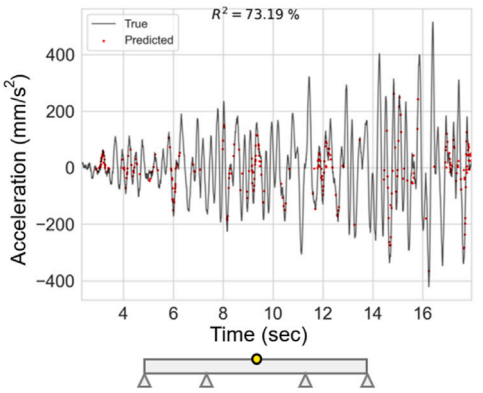

(b) A sample VFSN at mid-span of the bridge.

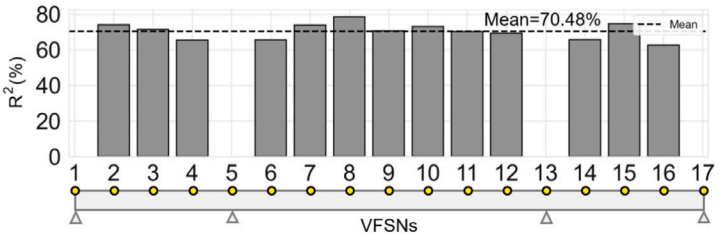

(c) R^2 value for the predicted acceleration responses at VFSNs.

Fig. 13. Comparison of the predicted acceleration response for two sample VFSNs and R^2 for all the VFSNs (using residual CP response).

Table 3
Comparison of exact and identified frequencies (considering road roughness).

True freqs (Hz)	Identified freqs (Hz)	Relative error (%)
1.44	1.41	2.2
3.68	3.71	0.7
4.66	4.67	0.14

$$\mathrm{MAC}(\phi_{\mathrm{identified}}, \phi_{\mathrm{true}}) = \frac{|\phi^T_{\mathrm{identified}} \phi_{\mathrm{true}}|^2}{(\phi^T_{\mathrm{identified}} \phi_{\mathrm{identified}})(\phi^T_{\mathrm{true}} \phi_{\mathrm{true}})} \times 100 \tag{39}$$

where $f_{\mathrm{identified}}$ and f_{true} refer to the identified and true natural frequencies of the structure, respectively. Similarly, $\phi_{\mathrm{identified}}$ and ϕ_{true} represent the identified and corresponding true mode shapes, respectively.

It should be noted that while MAC is employed in this study solely to evaluate the quality of the identified mode shapes, it can be further adapted or transformed for damage detection. For instance, applying a logarithmic-based damage index like $\left[-1/\log(1-\mathrm{MAC})\right]$ can amplify small deviations from MAC=1, thereby improving sensitivity to moderate stiffness reductions.

5. Discussion on influencing factors

In this section, the effects of various influencing factors on the framework's response prediction and modal identification accuracy are investigated and discussed. Unless otherwise specified, all investigations are conducted under consistent conditions: road roughness Type A, a 5% measurement noise level, and a baseline setup. The baseline configuration consists of two sensing agents, 17 VFSNs, and a base speed of 25 m/s. For clarity, in all figures and plots presented in this section, mode shape error and response prediction error are expressed as percentages of (100 – MAC) and (100 – R^2), respectively.

The missing rate in this context is defined as follows: when at least two MSNs are near a VFSN, the predicted responses at the VFSN are valid and demonstrate high accuracy. However, when the mobile sensors move beyond the vicinity of a VFSN, and it is

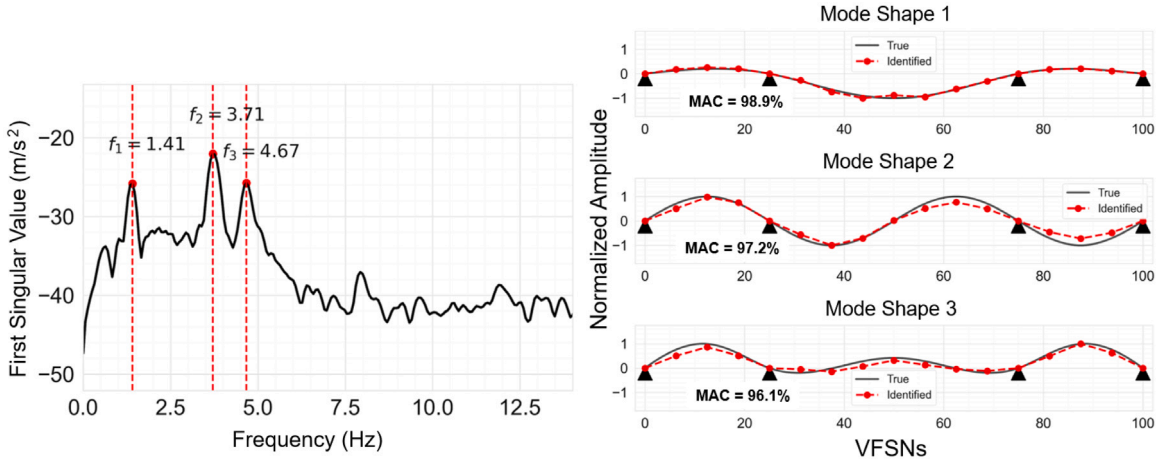

(a) First singular value of the PSD matrix based. (b) Identified mode shapes of the bridge.

Fig. 14. Modal identification results using FDD on the predicted acceleration responses with missing values (considering road roughness).

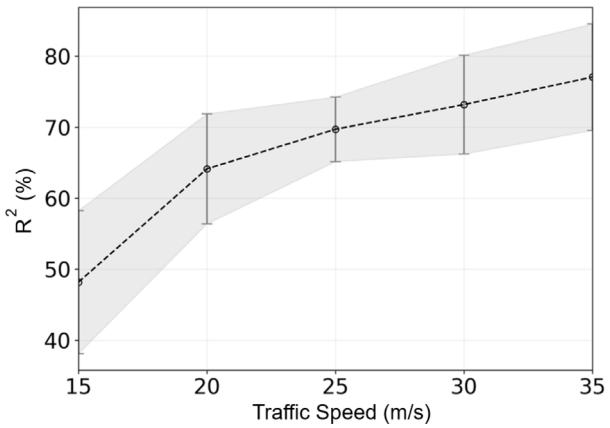

Fig. 15. Effect of traffic speed on the mean accuracy of predicted acceleration responses for VFSNs (mean ± STD of the accuracies is also shown).

no longer positioned between two MSNs, the mapping error increases significantly compared to the ground truth. Intervals where the VFSN is not between two MSNs are classified as "missing regions", while those where the VFSN remains between two sensors are termed "scanned regions". The missing rate is calculated as the ratio of data points in missing regions to the total signal length, averaged across all VFSNs.

5.1. Traffic speed

To study the sensitivity of the proposed framework to traffic speed, five different values were considered (15, 20, 25, 30, 35 m/s). Numerical simulations in OpenSees were repeated for each traffic speed, keeping all other variables constant (e.g., road roughness, measurement length, number of VFSNs, and sensing agents). As shown in Fig. 15, increasing traffic speed improves the R^2 accuracy and mode shape identification due to the numerical differentiation concept mentioned in Section 2.4. Fig. 16 summarizes the sensitivity analysis of the identified natural frequencies and mode shapes to traffic speed. Higher modes are identified more accurately at higher speeds, as the higher traffic speeds can excite the bridge's higher frequencies. However, when the traffic speed is around 15 m/s, the modal identification error is notably high, especially for the third mode. To address this issue in real-world scenarios, data collection can be limited to periods when the average traffic speed exceeds 25 m/s, disregarding data from slower traffic conditions.

5.2. Number of selected sensing agents effect

As shown in Fig. 17(a), increasing the number of sensing agents slightly reduces the error in response prediction. This improvement occurs because additional data from more agents enhances the model's ability to monitor the bridge comprehensively,

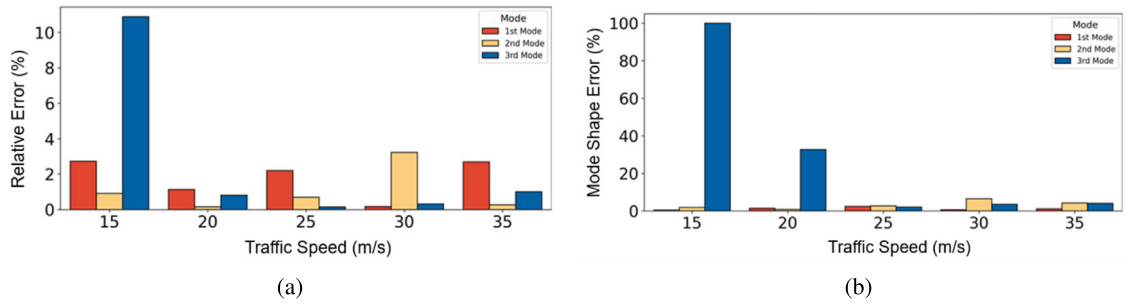

Fig. 16. Sensitivity of the modal identification results to traffic speed variations: (a) Relative error of the natural frequencies, and (b) Error of the mode shapes.

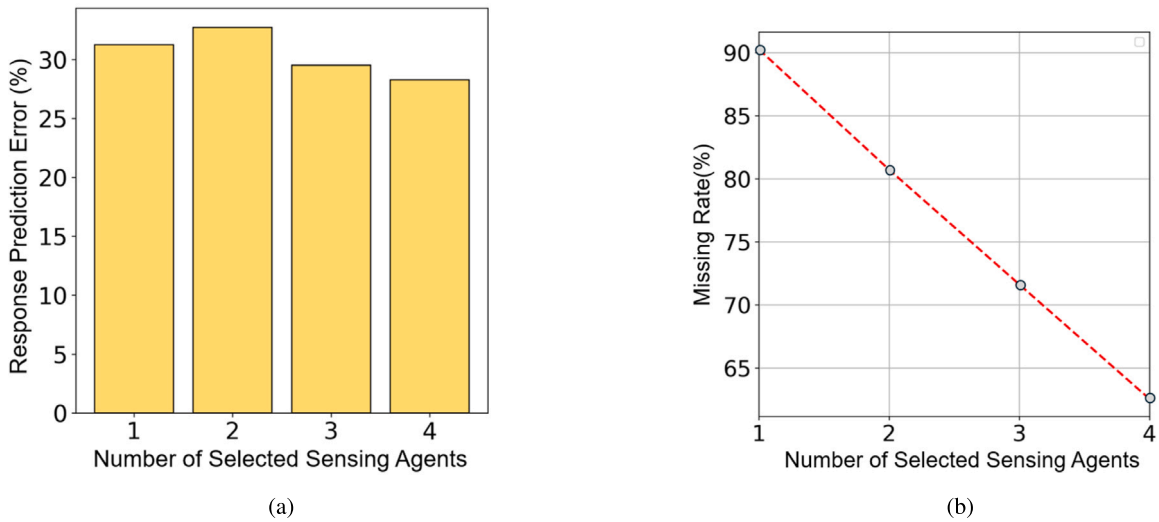

Fig. 17. Impact of the number of sensing agents on response prediction. (a) Mean response prediction error (over all VFSNs) vs. the number of sensing agents. (b) Mean missing rate of the bridge response matrix (over all VFSNs) vs. the number of sensing agents.

thereby minimizing prediction errors. Furthermore, Fig. 17(b) illustrates that the missing data ratio, representing the proportion of unscanned region of the bridge response matrix, decreases when more sensing agents are utilized. This reduction is attributed to the higher density of sensing nodes available at any given time.

Additionally, Fig. 18 investigates the effect of the number of sensing agents on mode shape identification error (100 − MAC). The error decreases for all three mode shapes (except the first one) as more sensing agents are used, with the case of a single sensing agent showing significantly higher error. Interestingly, it is also observed that the number of sensing agents does not significantly impact frequency identification results.

Overall, incorporating more sensing agents enhances the accuracy of response prediction as well as mode shape identification. It is crucial to keep the number of sensing agents as low as possible to maintain the robustness and feasibility of the proposed random mobile sensing method, particularly in practical scenarios where access to a large number of vehicles with internet connectivity may be limited. Based on numerical observations, selecting two sensing agents for the constant number of VFSNs is determined to be optimal.

5.3. Number of virtual fixed sensing nodes

This part investigates the effect of the number of selected VFSNs on response prediction error and modal identification error. Fig. 19(a) shows that increasing the number of VFSNs generally increases the mean response prediction error. Similarly, Fig. 19(b) indicates that the mean missing rate of the bridge response matrix increases with more VFSNs. This is because a higher number of VFSNs results in a smaller scanned region for each VFSN when the number of sensing agents remains constant, leading to densely distributed but minimally scanned areas.

Fig. 20 demonstrates that mode shape identification error also increases, especially for the first and third modes. Despite this, a minimum number of VFSNs is necessary to achieve sufficient spatial resolution for mode shapes, emphasizing the need to optimize

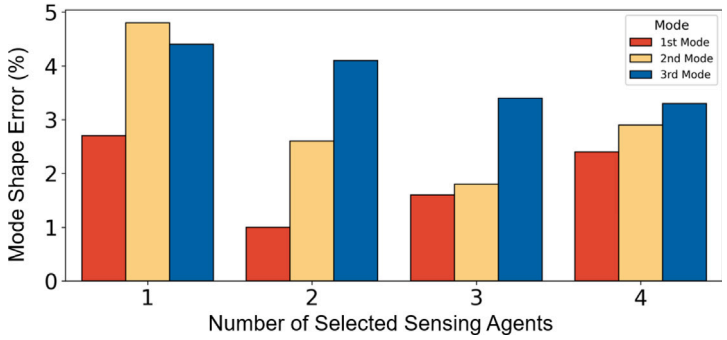

Fig. 18. Mode shape identification error versus the number of sensing agents.

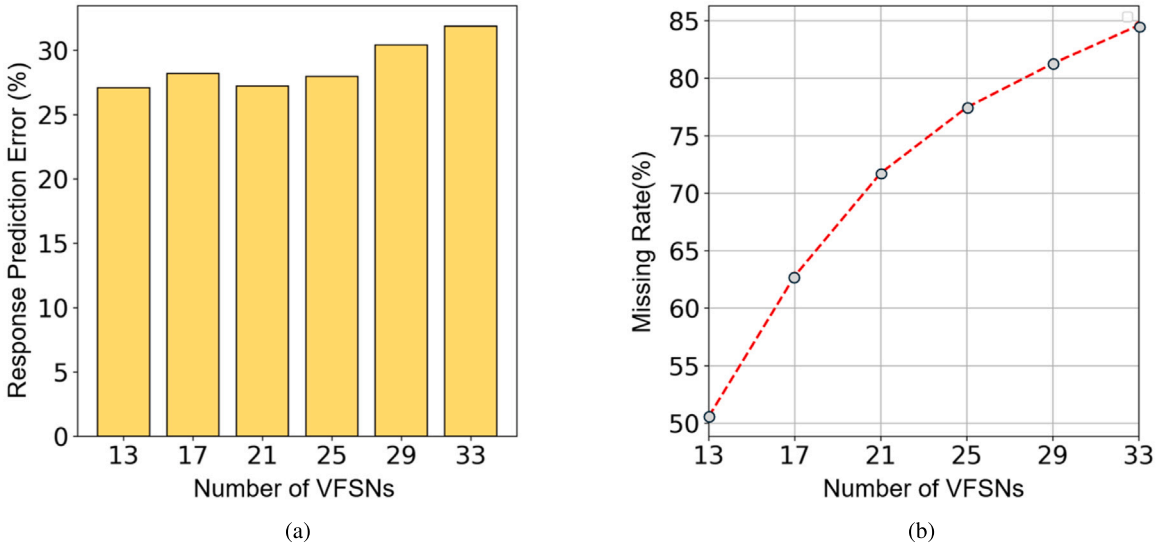

Fig. 19. Impact of the number of the selected VFSNs on response prediction results. (a) Mean response prediction error (over all VFSNs) vs. number of VFSNs. (b) Mean missing rate of the bridge response matrix (over all VFSNs) vs. number of VFSNs.

the number of VFSNs for balanced accuracy and efficiency. Similar to the effect of the number of sensing agents, the number of VFSNs does not impact frequency identification results. To achieve a denser spatial response prediction and mode shape identification, it is more effective to use different configurations of VFSNs at various locations rather than increasing their number. By running the framework with the desired number of VFSNs and combining the results from different configurations, prediction accuracy can be maintained. Based on observations in this research, 17 VFSNs have been selected as the base number.

5.4. Effect of data length on modal identification

To investigate how data length influences the quality of mode shape and frequency identification in our crowdsensing framework, we performed a supplementary test using subsets of the entire 15.64 s simulation (3127 points). We extracted portions ranging from 40% to 100% of the full dataset and carried out the same modal identification procedure.

Figs. 21(a) and 21(b) show that once the partial data length exceeds about 75% of the original signal, the MAC for Modes 1–3 remains above 95%, and the frequency errors remain below approximately 7% for the first mode and 1% for the higher modes. For shorter data windows (less than 65% of the base data length), MAC drops to under 90% for some modes, and frequency errors can exceed 10%. Hence, while the proposed framework places no explicit upper bound on data length, ensuring sufficiently long measurement time is beneficial for robust and accurate modal identification.

In conclusion, the analysis confirms that collecting more than 75% of the base data (in our case, roughly 11 s out of 15.64 s) yields minimal further improvement in MAC and frequency accuracy.

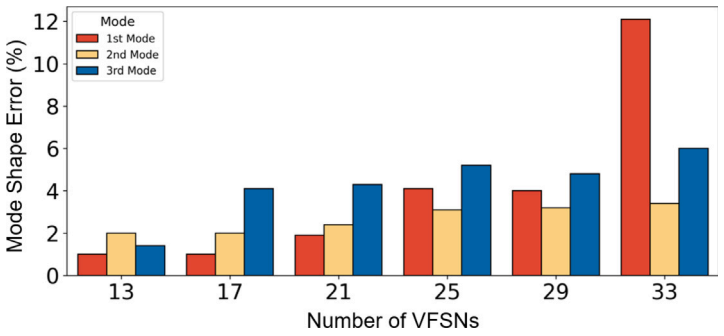

Fig. 20. Mode shape identification error versus the number of VFSNs.

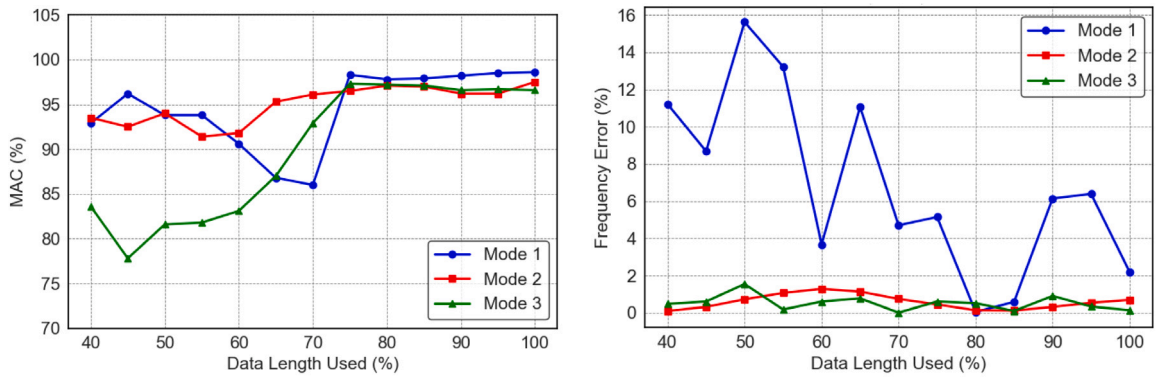

(a) MAC values for the first three modes.

(b) Absolute relative frequency error for each mode.

Fig. 21. Comparison of MAC values and absolute relative frequency error for different data dimensions from 40% to 100% of the base 3127 points.

5.5. Measurement noise

In real-world applications, when collecting acceleration data from vehicles, ambient noise is also captured. Therefore, investigating the effect of introducing noise-corrupted data into the framework is necessary to evaluate its robustness. Ambient noise is typically modeled as a random Gaussian process, and the original signals can be replicated using Eq. (40) [59]:

$$\mathbf{s_n} = \mathbf{s_o} + E_n.\sigma_o.\text{randn}(p) \tag{40}$$

Here, $\mathbf{s_n}$ represents the signals with added noise, $\mathbf{s_o}$ denotes the noise-free recorded accelerations, E_n represents the noise level, and σ_o represents the standard deviation of the signals. The function randn(p) generates p (signal length) random numbers following a standard normal distribution.

In this section, we examine the impact of noise levels ranging from 0% to 5% on the bridge response prediction results and modal identification results. As expected, Fig. 22(a) shows that the mean response prediction error of all VFSNs increases with higher noise levels. Notably, up to a noise level of 3%, the error introduced by ambient noise (relative to zero noise results) remains below 10%. This is significant because the framework does not incorporate noise cancellation during response prediction. This is because it is difficult to distinguish between noise and high-frequency components of the bridge response in real-world scenarios, and it is crucial to ensure that all necessary information is retained for further calculations.

Conversely, Fig. 22(b) indicates that the identified mode shapes are only slightly affected by ambient noise. This robustness is due to the effectiveness of the FDD method used for modal identification. The framework can identify the first three mode shapes with less than 3% error, even with noise levels up to 5%. Additionally, it is observed that ambient noise has almost no impact on frequency identification results. These findings demonstrate that the framework is robust to ambient noise.

5.6. Monte Carlo analysis

To determine whether the random selection of sensing agents affects the accuracy of bridge response prediction and mode shape identification, a Monte Carlo simulation was conducted by running the framework 30 times with different sets of randomly selected sensing agents. Fig. 23(a) illustrates the variability of the R^2 values for response prediction across various VFSNs. The data, confined

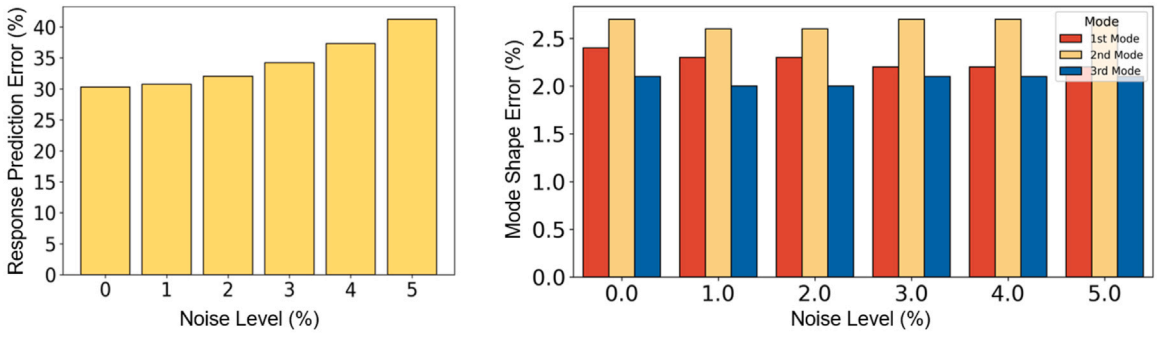

Fig. 22. Ambient noise effect on: (a) the mean bridge response prediction error, (b) the mode shape identification error.

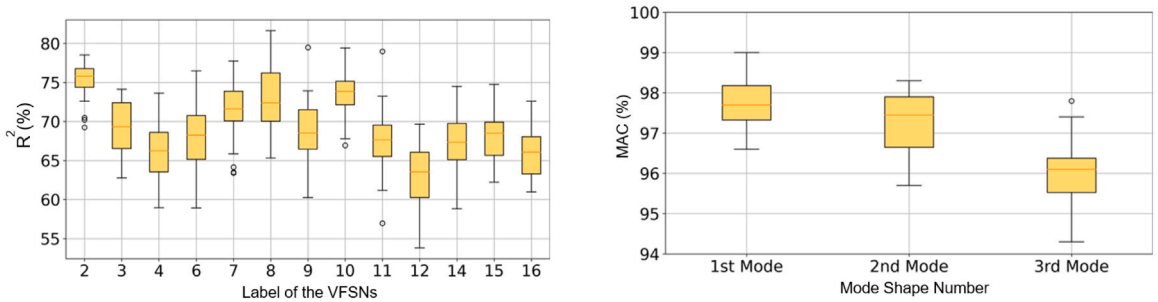

Fig. 23. Monte Carlo analysis of response prediction and mode shape identification under a random selection of sensing agents. (a) Variability of R^2 values across multiple VFSNs. (b) Variation in MAC for the first three mode shapes.

within a 95% confidence interval, indicates minimal impact on prediction accuracy, demonstrating the method's robustness against the specific choice of sensing agents. Similarly, Fig. 23(b) investigates the stability of the first three mode shapes' identification. The results, also within a 95% confidence interval, show that the accuracy (MAC) remains consistently above 95%. Although there is slight fluctuation, the frequency identification is largely unaffected by the random selection of agents.

5.7. Impact of variable traffic speed

As discussed in Section 2.4, the proposed framework assumes constant speeds and fixed wheel distances for the sensing agents to simplify the analysis. However, this assumption does not limit the method's applicability under real-world traffic conditions with variable vehicle speeds. The time step (Δt) in Eq. (28) serves as the numerical time step for the first-order backward Euler differentiation method and can adapt to individual sensing agents, as long as Δt remains sufficiently small to preserve numerical accuracy.

To evaluate the framework under variable traffic speeds, another vehicle–bridge simulation was conducted. Vehicles were assigned speeds uniformly distributed between 20 m/s and 30 m/s, based on a uniform probability distribution. To avoid unrealistic interactions, vehicles with higher speeds were positioned closer to the bridge during initialization. This ensured no collisions occurred during the simulation and maintained realistic traffic flow dynamics. Using this setup, the simulation was repeated with the variable speed scenario, and the processed acceleration responses of the bridge were used to estimate its modal properties. Preprocessing steps, including offset removal, were applied to the data before modal analysis. The identified modal shapes were then compared to the ground truth modal shapes of the bridge. The results indicate that the first and second modes remained largely unaffected by variable traffic speeds, showing strong agreement with the reference case under constant vehicle speed (25 m/s), as shown in Fig. 24. However, the third mode exhibited higher sensitivity to speed variations, likely due to the influence of varying time steps on numerical differentiation. Higher modes inherently show higher sensitivity to inaccuracies in temporal data.

6. Conclusions and future work

This paper has introduced an innovative mobile-sensing-based continuous monitoring framework for continuous indirect monitoring of bridge structures. This innovative system utilizes a randomly selected network of mobile sensors to estimate bridge

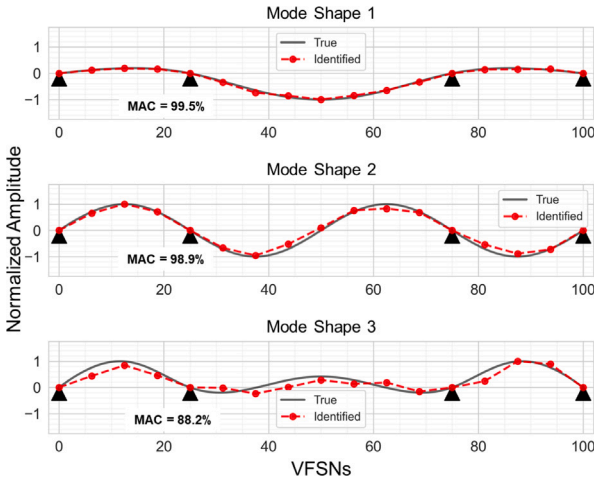

Fig. 24. Comparison of identified modal shapes for the first three modes of the bridge under variable traffic speeds (20–30 m/s) with the ground truth modes.

responses at some predetermined fixed sensing nodes on the bridge (VFSNs). Our method is initiated by gathering critical data from mobile sensors, including vertical acceleration, pitch rotation, and location data. This collected vibration data is subsequently transformed to the vehicles' contact points, where the pervasive effects of road roughness are effectively mitigated using calculated residual CP responses. These refined responses are then systematically correlated to VFSNs on the bridge through linear interpolation and regularized optimization. Even with a substantial data loss rate of 80%, common in traditional crowdsensing methods, this innovative framework effectively identifies the bridge's modal properties using a randomly sampled response matrix.

The effectiveness of our framework was validated by numerical data derived from detailed simulations of a three-span bridge subjected to dynamic traffic flow, carefully considering factors such as road roughness and the intricate dynamics of vehicle–bridge interactions. Remarkably, even with a substantial 80% rate of missing data and relying solely on just two mobile sensors in conjunction with 17 VFSNs, the proposed method demonstrated high accuracy in identifying the first three mode shapes and natural frequencies of the bridge, achieving MAC values exceeding 95% and maintaining relative errors below 3%.

Our study extensively evaluated key parameters influencing the proposed framework, including traffic speed, the number of sensing agents, VFSNs, ambient noise, random sensor selection using Monte Carlo simulations, and variable traffic speeds. The results confirmed the framework's resilience to ambient noise and reliable performance under random sensor selection conditions. The optimal configuration for operational efficiency was determined to include 2 sensing agents and 17 VFSNs. The findings further demonstrated that, with appropriate preprocessing, the method effectively identifies bridge modal properties in practical scenarios, even under speed variations ranging from 72 to 108 km/h.

However, the proposed framework has certain limitations. Its optimal performance is achieved at traffic speeds consistently exceeding 25 m/s, with accuracy potentially affected by greater variations in vehicle dynamics. Additionally, the framework requires access to a dataset of vehicle properties to identify contact point responses and relies on a well-designed data acquisition app for drivers' smartphones and a robust cloud processing server. Future research will aim to address these challenges by developing access to a more extensive database of vehicle parameters. Emphasis will be placed on the practical implementation and laboratory validation of the framework. Additional investigations will focus on adapting to variations in vehicle properties, managing asynchronous data collection across vehicles, and analyzing the effects of variable traffic speeds in greater detail. These efforts seek to improve the system's practicality and reliability for real-world bridge monitoring, ultimately advancing the development of smart and resilient urban infrastructure.

CRediT authorship contribution statement

Mohammad Talebi-Kalaleh: Writing – original draft, Visualization, Methodology, Investigation, Formal analysis, Data curation, Conceptualization. **Mustafa Gül:** Writing – review & editing, Validation, Supervision, Methodology, Conceptualization. **Qipei Mei:** Writing – review & editing, Validation, Supervision, Resources, Project administration, Methodology, Funding acquisition, Conceptualization.

Declaration of Generative AI and AI-assisted technologies in the writing process

During the preparation of this work, the authors used Grammerly in order to improve writing. After using this tool, the authors reviewed and edited the content as needed and take full responsibility for the content of the publication.

Declaration of competing interest

The authors declare that they have no known competing financial interests or personal relationships that could have appeared to influence the work reported in this paper.

Acknowledgments

This research was supported in part by the Natural Sciences and Engineering Research Council of Canada (NSERC) through the Discovery Grant (RGPIN-2022-04160) and Alliance Grant (ALLRP 576826–22).

Data availability

Data will be made available on request.

References

[1] Statistics Canada, Canada's Core Public Infrastructure Survey: Roads, Bridges and Tunnels, Technical Report, Canada's National Statistical Agency, 2020.
[2] Z. Lounis, Aging Highway Bridges, Technical Report, Institute for Research in Construction, National Research Council Canada, 2007.
[3] Parsons Brinckerhoff and Engineering and Industrial Heritage, NCHRP Project 25-25, Task 15: A Context For Common Historic Bridge Types, The National Cooperative Highway Research Program, Transportation Research Council, National Research Council, 2005, Prepared for The National Cooperative Highway Research Program.
[4] Canadian Construction Association, Canadian Public Works Association, Canadian Society for Civil Engineering, Federation of Canadian Municipalities, Informing the Future: Assessing the Health of Our Communities' Infrastructure. Canadian Infrastructural Rep. Card 2019, Technical Report, Canadian Infrastructure Report Card (CIRC), Ottawa, Canada, 2019.
[5] Federal Highway Administration, Deficient bridges by highway system 2016, 2016, https://www.fhwa.dot.gov/bridge/nbi/no10/defbr16.cfm. (Accessed 27 June 2024).
[6] Z. Deng, M. Huang, N. Wan, J. Zhang, The current development of structural health monitoring for bridges: A review, Buildings 13 (6) (2023) 1360.
[7] R. Niyirora, W. Ji, E. Masengesho, J. Munyaneza, F. Niyonyungu, R. Nyirandayisabye, Intelligent damage diagnosis in bridges using vibration-based monitoring approaches and machine learning: A systematic review, Results Eng. 16 (2022) 100761.
[8] M. Flah, I. Nunez, W. Ben Chaabene, M.L. Nehdi, Machine learning algorithms in civil structural health monitoring: A systematic review, Arch. Comput. Methods Eng. 28 (2021) 2621–2643.
[9] Emin Aktan, Ivan Bartoli, Branko Glišić, Carlo Rainieri, Lessons from bridge structural health monitoring (SHM) and their implications for the development of cyber-physical systems, Infrastructures 9 (2) (2024).
[10] A. Malekjafarian, P.J. McGetrick, E.J. OBrien, A review of indirect bridge monitoring using passing vehicles, Shock. Vib. 2015 (2015) e286139.
[11] Y.B. Yang, C.W. Lin, J.D. Yau, Extracting bridge frequencies from the dynamic response of a passing vehicle, J. Sound Vib. 272 (3–5) (2004) 471–493.
[12] Abdollah Malekjafarian, Robert Corbally, Wenjie Gong, A review of mobile sensing of bridges using moving vehicles: Progress to date, challenges and future trends, Structures 44 (2022) 1466–1489.
[13] Chengjun Tan, Ahmed Elhattab, Nasim Uddin, "Drive-by"bridge frequency-based monitoring utilizing wavelet transform, J. Civ. Struct. Heal. Monit. 7 (2017) 615–625.
[14] Chengjun Tan, Nasim Uddin, Hilbert transform based approach to improve extraction of" drive-by" bridge frequency, Smart Struct. Syst. 25 (3) (2020).
[15] William Locke, Justin Sybrandt, Laura Redmond, Ilya Safro, Sez Atamturktur, Using drive-by health monitoring to detect bridge damage considering environmental and operational effects, J. Sound Vib. 468 (2020) 115088.
[16] Chengjun Tan, Drive-by bridge monitoring and damage detection, 2019.
[17] X. Kong, C.S. Cai, B. Kong, Numerically extracting bridge modal properties from dynamic responses of moving vehicles, J. Eng. Mech. 142 (2016) 1–12.
[18] Y.B. Yang, Y.C. Li, K.C. Chang, Constructing the mode shapes of a bridge from a passing vehicle: A theoretical study, Smart Struct. Syst. 13 (2014) 797–819.
[19] T.J. Matarazzo, I. Dabbaghchian, L. Cronin, S.N. Pakzad, S.S. Eshkevari, H. Yin, R. Lassman, P. Santi, C. Ratti, Quality analyses of crowdsourced smartphone trips for bridge dynamic monitoring, in: Life-Cycle of Structures and Infrastructure Systems, CRC Press, 2023, pp. 825–832.
[20] Jiantao Li, Xinqun Zhu, Jian Guo, Enhanced drive-by bridge modal identification via dual Kalman filter and singular spectrum analysis, Struct. Control. Heal. Monit. 29 (5) (2022) e2927.
[21] Zhen Peng, Jun Li, Hong Hao, Ning Yang, Mobile crowdsensing framework for drive-by-based dense spatial-resolution bridge mode shape identification, Eng. Struct. 292 (2023) 116515.
[22] Mohammad Talebi-Kalaleh, Qipei Mei, A novel drive-by system identification approach for bridges utilizing a modal FRF similarity criterion and soft-imputing, in: International Conference on Experimental Vibration Analysis for Civil Engineering Structures, Springer, 2023, pp. 275–283.
[23] Qipei Mei, Nima Shirzad-Ghaleroudkhani, Mustafa Gül, S. Farid Ghahari, Ertugrul Taciroglu, Bridge mode shape identification using moving vehicles at traffic speeds through non-parametric sparse matrix completion, Struct. Control. Heal. Monit. 28 (7) (2021) e2747.
[24] Y. Zhang, L. Wang, Z. Xiang, Damage detection by mode shape squares extracted from a passing vehicle, J. Sound Vib. 331 (2012) 291–307.
[25] Y. Zhang, S.T. Lie, Z. Xiang, Damage detection method based on operating deflection shape curvature extracted from dynamic response of a passing vehicle, Mech. Syst. Signal Process. 35 (2013) 238–254.
[26] Z. Peng, J. Li, H. Hao, Development and experimental verification of an IoT sensing system for drive-by bridge health monitoring, Eng. Struct. 293 (2023) 116705.
[27] Debasish Jana, Satish Nagarajaiah, Full-field vibration response estimation from sparse multi-agent automatic mobile sensors using formation control algorithm, Sensors 23 (18) (2023).
[28] Xuefeng Zhao, Kwang Ri, Ruicong Han, Yan Yu, Mingchu Li, Jinping Ou, Experimental research on quick structural health monitoring technique for bridges using smartphone, Adv. Mater. Sci. Eng. 2016 (1) (2016) 1871230.
[29] Ekin Ozer, Rolands Kromanis, Smartphone prospects in bridge structural health monitoring, a literature review, Sensors 24 (11) (2024) 3287.
[30] Chul-Woo Kim, M. Kawatani, Challenge for a drive-by bridge inspection, in: Proceedings of the 10th International Conference on Structural Safety and Reliability, 2009, pp. 758–765.
[31] Abdollah Malekjafarian, Callum Moloney, Fatemeh Golpayegani, Drive-by bridge health monitoring using multiple passes and machine learning, in: European Workshop on Structural Health Monitoring: Special Collection of 2020 Papers-Volume 1, Springer, 2021, pp. 695–703.

[32] Qipei Mei, Mustafa Gül, A crowdsourcing-based methodology using smartphones for bridge health monitoring, Struct. Heal. Monit. 18 (5) (2019) 1602–1619.
[33] Mohammad Talebi-Kalaleh, Qipei Mei, Damage detection in bridge structures through compressed sensing of crowdsourced smartphone data, Struct. Control. Heal. Monit. 2024 (2024) 1–23.
[34] Thomas J. Matarazzo, Paolo Santi, Shamim N. Pakzad, Kristopher Carter, Carlo Ratti, Babak Moaveni, Chris Osgood, Nigel Jacob, Crowdsensing framework for monitoring bridge vibrations using moving smartphones, Proc. IEEE 106 (4) (2018) 577–593.
[35] Thomas J. Matarazzo, Dániel Kondor, Sebastiano Milardo, Soheil S. Eshkevari, Paolo Santi, Shamim N. Pakzad, Markus J. Buehler, Carlo Ratti, Crowdsourcing bridge dynamic monitoring with smartphone vehicle trips, Commun. Eng. 1 (1) (2022) 29.
[36] Kai Xue, Tomonori Nagayama, Boyu Zhao, Road profile estimation and half-car model identification through the automated processing of smartphone data, Mech. Syst. Signal Process. 142 (2020) 106722.
[37] Y.B. Yang, Bin Zhang, Tianyi Wang, Hao Xu, Yuntian Wu, Two-axle test vehicle for bridges: Theory and applications, Int. J. Mech. Sci. 152 (2019) 51–62.
[38] Michael E. Taylor, Introduction to differential equations, first ed., in: Pure and Applied Undergraduate Texts, vol. 14, American Mathematical Society, Providence, RI, 2011, p. 409, Hardcover, eBook, Hardcover + eBook.
[39] Y.B. Yang, B.Q. Wang, Z.L. Wang, K. Shi, H. Xu, B. Zhang, Y.T. Wu, Bridge surface roughness identified from the displacement influence lines of the contact points by two connected vehicles, Int. J. Struct. Stab. Dyn. 20 (14) (2020) 2043003.
[40] Kai Xue, Tomonori Nagayama, Boyu Zhao, Road profile estimation and half-car model identification through the automated processing of smartphone data, Mech. Syst. Signal Process. 142 (2020) 106722.
[41] Y.B. Yang, Baoquan Wang, Zhilu Wang, Kang Shi, Hao Xu, Scanning of bridge surface roughness from two-axle vehicle response by EKF-UI and contact residual: Theoretical study, Sensors 22 (9) (2022).
[42] Rajdip Nayek, Sriram Narasimhan, Extraction of contact-point response in indirect bridge health monitoring using an input estimation approach, J. Civ. Struct. Heal. Monit. 10 (5) (2020) 815–831.
[43] Y.-B. Yang, Z. Li, Z.-L. Wang, S.-M. Hsieh, A novel frequency-free movable test vehicle for retrieving modal parameters of bridges: theory and experiment, Mech. Syst. Signal Process. 170 (2022) 108854.
[44] Y.B. Yang, B. Zhang, Y. Qian, Y. Wu, Contact-point response for modal identification of bridges by a moving test vehicle, Int. J. Struct. Stab. Dyn. 18 (05) (2018) 1850073.
[45] R. Corbally, A. Malekjafarian, Examining changes in bridge frequency due to damage using the contact-point response of a passing vehicle, J. Struct. Integr. Maint. 6 (3) (2021) 148–158.
[46] H. Wang, T. Nagayama, J. Nakasuka, B. Zhao, D. Su, Extraction of bridge fundamental frequency from estimated vehicle excitation through a particle filter approach, J. Sound Vib. 428 (2018) 44–58.
[47] Y.B. Yang, H. Xu, Z.L. Wang, K. Shi, Using vehicle–bridge contact spectra and residue to scan bridge's modal properties with vehicle frequencies and road roughness eliminated, Struct. Control. Heal. Monit. 29 (8) (2022) Article ID e2968.
[48] Y. He, J.P. Yang, Z. Yan, Enhanced identification of bridge modal parameters using contact residuals from three-connected vehicles: theoretical study, Structures 54 (2023) 1320–1335.
[49] A. González, E.J. OBrien, P.J. McGetrick, Identification of damping in a bridge using a moving instrumented vehicle, J. Sound Vib. 331 (18) (2012) 4115–4131.
[50] Mohammad Talebi-Kalaleh, Qipei Mei, A mobile sensing framework for bridge modal identification through an inverse problem solution procedure and moving-window time series models, Sensors 23 (11) (2023).
[51] J. Kim, J.P. Lynch, J.-J. Lee, C.-G. Lee, Truck-based mobile wireless sensor networks for the experimental observation of vehicle–bridge interaction, Smart Mater. Struct. 20 (6) (2011) 065009.
[52] G. Michel Guzman-Acevedo, G. Esteban Vazquez-Becerra, Jesus R. Millan-Almaraz, Hector E. Rodriguez-Lozoya, Alfredo Reyes-Salazar, J. Ramon Gaxiola-Camacho, Carlos A. Martinez-Felix, GPS, Accelerometer, and Smartphone Fused Smart Sensor for SHM on Real-Scale Bridges, Adv. Civ. Eng. 2019 (2019) 6429430.
[53] Abdollah Malekjafarian, Patrick J. McGetrick, Eugene J. OBrien, A review of indirect bridge monitoring using passing vehicles, Shock. Vib. 2015 (2015) 286139, Publisher: Hindawi Publishing Corporation.
[54] Debasish Jana, Satish Nagarajaiah, Full-field vibration response estimation from sparse multi-agent automatic mobile sensors using formation control algorithm, Sensors 23 (18) (2023) 7848.
[55] Esther-Lydia Silva-Ramírez, Rafael Pino-Mejías, Manuel López-Coello, María-Dolores Cubiles-de-la Vega, Missing value imputation on missing completely at random data using multilayer perceptrons, Neural Netw. 24 (1) (2011) 121–129, Epub 2010 Sep 17.
[56] Qipei Mei, Mustafa Gül, A crowdsourcing-based methodology using smartphones for bridge health monitoring, Struct. Heal. Monit. 18 (2019) 1602–1619.
[57] J. Li, K.A. Mechitov, R.E. Kim, B.F. Spencer, Efficient time synchronization for structural health monitoring using wireless smart sensor networks, Struct. Control. Heal. Monit. 23 (3) (2016) 470–486.
[58] Ashish Shrestha, Ji Dang, Xin Wang, Shogo Matsunaga, Smartphone-Based Bridge Seismic Monitoring System and Long-Term Field Application Tests, J. Struct. Eng. 146 (2) (2020) 04019208.
[59] Rune Brincker, Lingmi Zhang, Palle Andersen, Modal identification of output-only systems using frequency domain decomposition, Smart Mater. Struct. 10 (2001) 441–445.
[60] F. McKenna, G.L. Fenves, M.H. Scott, Open system for earthquake engineering simulation, 2000, University of California, Berkeley.
[61] Arturo Gonzalez, Vehicle-bridge dynamic interaction using finite element modelling, in: David Moratal (Ed.), Finite Element Analysis, IntechOpen, Rijeka, 2010.
[62] M. Talebi-Kalaleh, Q. Mei, Toward indirect real-time prediction of bridge vibration responses under traffic flow through a population of connected sensing vehicles, in: Proceedings of the 11th European Workshop on Structural Health Monitoring, EWSHM 2024, 2024.
[63] Yuefeng Shao, Changqing Miao, J.M.W. Brownjohn, Youliang Ding, Vehicle-bridge interaction system for long-span suspension bridge under random traffic distribution, Structures 44 (2022) 1070–1080.
[64] ISO 8608: Mechanical Vibration–Road Surface Profiles–Reporting of Measured Data, 1995, International Standardization Organization.